THE JOURNAL OF THE

ASTRONAUTICAL SCIENCES

VOLUME VII, NO. 1 SPRING 1960

CONTENTS

PUBLISHED BY THE AMERICAN ASTRONAUTICAL SOCIETY, INC.

THE AMERICAN ASTRONAUTICAL SOCIETY, INC.

516 Fifth Avenue, New York 36, New York, U.S.A.

THE AMERICAN ASTRONAUTICAL SOCIETY

The American Astronautical Society, founded in 1953 and incorporated in New York State in 1954, is a national scientifi organization dedicated to advancement of the astronautical sciences. The society considers manned interplanetary space fligh a logical progression from today's high-performance research aircraft, guided missile, and earth satellite operations. The scop of the society is illustrated by a partial list of the astronautical fields of interest: astronavigation, biochemistry, celestial me chanics, cosmology, geophysics, space medicine, and upper atmosphere physics, as well as the disciplines of astronautical engineerin including space vehicle design, communications, control, instrumentation, guidance, and propulsion. The aims of the societ are to encourage scientific research in all fields related to astronautics and to propagate knowledge of current advances. Promotio of astronautics in this way is accomplished by the society largely through its program of technical meetings and publication

AFFILIATIONS

AAS cooperates with other national and international scientific and engineering organizations. AAS is an affiliate of the Ameri can Association for the Advancement of Science and a member organization of the International Astronautical Federation.

MEMBERSHIP REQUIREMENTS

All persons having a sincere interest in astronautics or engaged in the practice of any branch of science, which contributes to or advances the astronautical sciences, are eligible for one of the various grades of membership in the Society. Requirements are tabulated below. A special category of Student Membership has been authorized for full time students or those under 18 years of age. A nominal membership fee of $5.00 is made in such cases to cover publication costs. The Directors of the Society may elect as Fellows of the Society those who have made direct and significant contributions to the astronautical sciences. Information regarding individual membership as well as Corporate and Benefactor Membership may be obtained by writing the Corresponding Secretary at the Society address.

Grade	Contribution To Astronautics	Experience or Scientific Training*	Annual Dues
Affiliate Member	Interest	none required	$8
Associate Member	Direct Interest	4 years	$10
Member	Active Interest	8 years	$10
Senior Member	Recognized Standing and Direct Contribution	10 years	$15

* A Bachelor's, Master's or Doctor's degree in any branch of science or engineering is equivalent to four, six or eight years of experience, respectively.

JOURNAL OF THE
ASTRONAUTICAL SCIENCES
Director of Publications, Ross Fleisig
Editor, Robert E. Roberson
Associate Editor, Charles H. Moss
Assistant Editor, Carl A. DuNah, Jr.
Circulation Manager, George Clark
Address all Journal correspondence to
Box 24721, Los Angeles 24, Calif.

Subscription Rates: One year $5.00; foreig $6.00; single copy $1.25. The Journal is pub lished quarterly and sent without charge t members of the Society.

Long Range Detection by Star Occultation*

Harvey Dubner†

ntroduction

This paper briefly presents the "Star Occultation" echnique for providing long range detection of objects 1 space (such as satellites and other space vehicles). 'he basic principle involved is that an object moving in pace must eventually pass between the observer and ome stars; that is, the body occults the light from these tars. Thus, the term "star occultation". The angular osition and time of these occultations are used to etermine accurately orbits of objects in space.

This technique was originally conceived for ground-o-air operation; however, it was ineffective in the day-ime and quite limited for nighttime usage due to atmos-heric effects (such as star twinkling). With the advent f the space age, an observation platform can now be istalled above the atmosphere so that this technique or long range detection by star occultation becomes iteresting.

The capabilities, instrumentation and limitations of his technique are discussed. Detection ranges of over 0,000 miles are possible; and in one example, 120,000 iles is shown to be feasible.

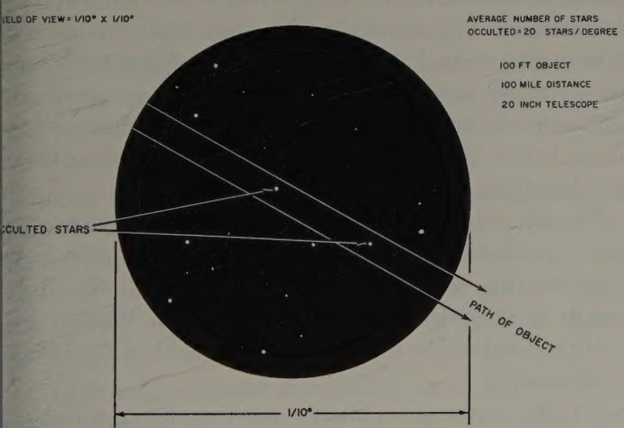

Fig. 1. Detection by Star Occultation

Figure 1 illustrates the basic principle and presents a mple example of star occultation; in this case, two ccultations have taken place in $\frac{1}{10}$ degree of motion.

stronomical Data

The study of star occultation techniques began with e compilation of data relating to the number, density id distribution of stars as a function of their bright-

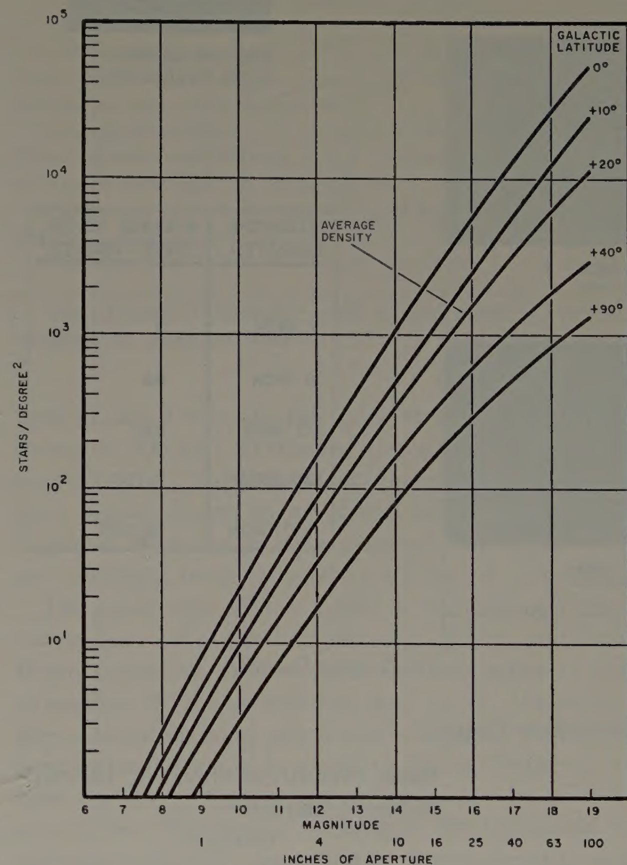

Fig. 2. Visual Star Density

ness. The Milky Way conveniently serves as the galactic equator with all galactic latitudes chosen in proper relation to this reference.

The relationship between density and galactic latitude is shown in Fig. 2, a graph of star density (star/degree²) as a function of telescope aperture and star magnitude. The 10, 20, 40 and 90 degree curves represent the densities observed at these latitudes. The 20° curve represents the average density of the overall galaxy. The graph illustrates that star density is approximately linear with telescope area in the vicinity of 13th magnitude stars. To emphasize the information obtained in the graph shown in Fig. 2, several significant points on the 20° curve were selected and translated on to the pictorial display shown in Fig. 3.

The average number of stars occulted per degree of motion is a function of the effective telescope diameter, the linear breadth of the object (transverse to the line of motion) and distance. Examples are tabulated in Table 1 from the basic formula,

* Revised version of paper presented at the 5th Annual eeting of the AAS, Washington, D. C., December 1958.
† Avion Division, ACF Industries, Incorporated, Paramus, ew Jersey.

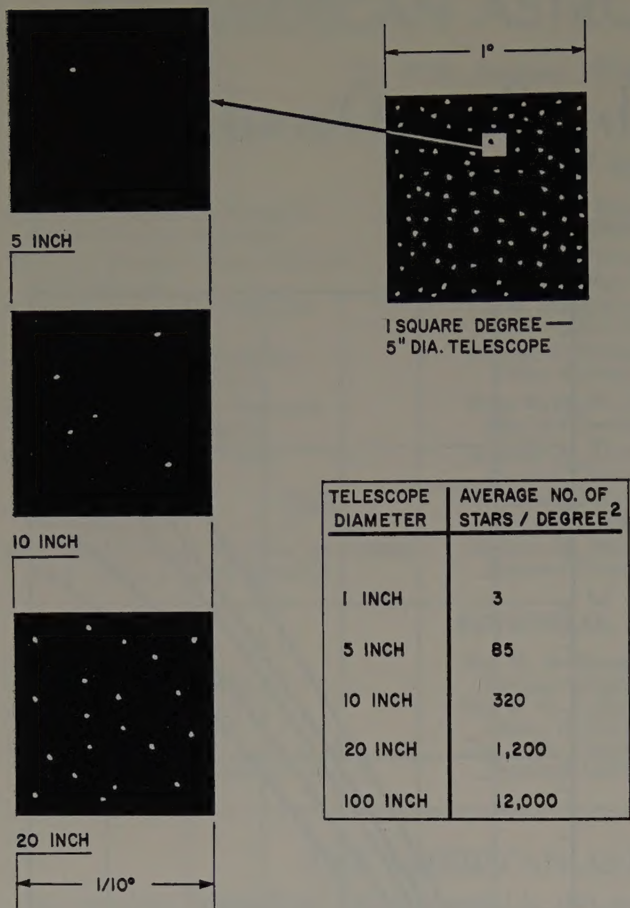

TELESCOPE DIAMETER	AVERAGE NO. OF STARS / DEGREE^2
1 INCH	3
5 INCH	85
10 INCH	320
20 INCH	1,200
100 INCH	12,000

Fig. 3. Star Density

Occultation/degree

$$= \frac{\text{linear breadth of object} \times \text{effective telescope diameter}}{\text{distance}}$$

TABLE 1

Average Number of Occultations

Linear Breadth of Object Size	Distance	Effective Telescope Diameter	Average Occultations Per Degree
10 ft.	200 miles	20 inch	1
		100 inch	10
	2000 miles	20 inch	.1
		100 inch	1
100 ft.	200 miles	20 inch	10
		100 inch	100
	2000 miles	20 inch	1
		100 inch	10

Instrumentation

The proposed means for implementing the star-occultation technique consists of a telescope, a detector, a storage and comparator device, a clock, and a computer. (The computer would most likely be earthbound.

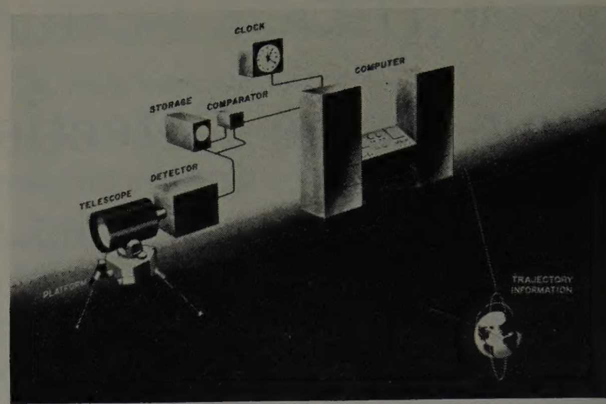

Fig. 4. Instrumentation

Thus a data link for telemetering the data would be necessary.)

Figure 4 shows a telescope mounted on a platform which is space-stabilized by optically slaving it to two reference stars.* A satellite or space station would serve as a suitable platform. Transferring the view from the telescope to a practical electrical output is accomplished by an integrating image tube such as an image intensifier orthicon. The electrical output is then stored for comparison with the next frame to determine the occurrence and location of occultations. Occultation location and time are fed to a computer in which orbits and trajectories are calculated.

Telescope.—The telescope collects the light energy from each star and focuses it on the detector. The telescope must have a suitable degree of resolution for the accurate identification of a star. Referring to Fig. 3, it can be seen that for a 20-inch telescope stars have an average spacing of about $\frac{1}{30}$ of a degree. The telescope resolution would therefore not have to be much better than 1 minute of arc to determine which star has been occulted.

The 20-inch telescope normally used by astronomers has a resolution of about $\frac{1}{5}$ second of arc which far exceeds this requirement. Consequently the focal length of the telescope can be decreased, thereby permitting a reduction in the size and weight of the overall equipment.

On the basis of available data and equipment, it appears that an f/1 concentric telescope would be sufficient to achieve the desired resolution over large fields of view.

Detector.—The detector is used to convert the light energy to its electrical equivalent. Investigations of available devices for converting light to its electrical analog have indicated that the image intensifier orthicon developed by RCA fulfills the essential requirements of a detector. Its potential sensitivity is six times better than the human eye, and its resolution is 100 lines per inch, which is adequate. Present models of this orthicon have a sensitive surface that measure

* Only two stars are required to establish a reference.

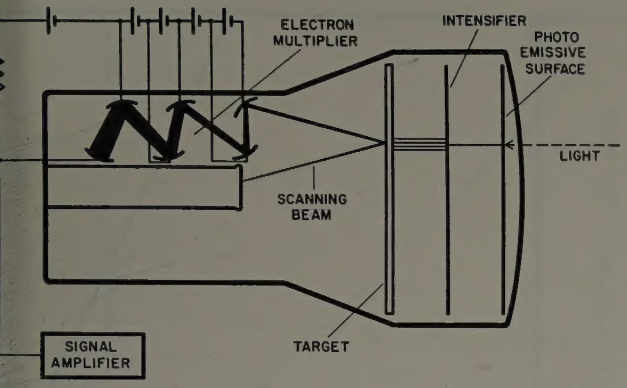

FIG. 5. Image Intensifier Orthicon

.6 inches x 1.6 inches. However, RCA states that ırger sizes can be produced.

Figure 5 illustrates the basic operation of a detector. tarting with the light energy striking the photomissive surface (cathode), electrons are emitted which re attracted to the intensifier due to its high potential. ach electron, in bombarding the intensifier surface at igh velocity, dislodges several other electrons from is surface. These secondary electrons, in turn, strike e target surface. Scanning is then performed on the ther side of the target surface in the same manner as an ordinary orthicon and amplified in a conventional ype of multiplier. Internal noise in this orthicon is low nough so that individual photons can be counted.

For optimum sensitivity, frame time should be bout equal to the time of occultation. Considering e case of a 10-foot object traveling at an orbiting elocity of 20,000 feet per second, occultation time would e $\frac{1}{2000}$ second. This presents a problem which would ave to be solved by the use of several detectors in arallel.

Storage unit and comparator.—Determining when an ccultation has occurred would be accomplished by ame-to-frame comparison of star locations within the lescopic view. Considering the nature of the necessary ta, the use of electronic storage tubes seems to be the gical choice.

Storage tubes capable of handling up to 250,000 cometely isolated bits are now available; writing and ading rates up to 500 frames per second have been sed. Two storage channels are being considered for is system—one for writing the incoming information d the other for comparison with it. Comparison ould then be effected by the process of simple subaction, with the resulting occultation information ing fed to the computer.

Computer.—A digital computer would be employed r the calculation of orbits and trajectories. Since the tical resolution selected is consistent with star spacg, information fed to the computer will be accurate time but only approximate in angular data. Hence e computer must store information of star locations within its memory if it is to provide angular data with an accuracy in the order of fractions of a second of arc, as are desirable in computing trajectories.

As an example of the accuracy attainable, consider a satellite in a circular orbit as it passes directly overhead. Only two occultations are required to derive its

TABLE 2

Occultation Technique Accuracy

h = Distance from earth	200 mi.	2000 mi.
Time for one revolution	91 min.	156 min.
Maximum time orbit is visible from earth's surface	9 min.	41 min.
Time between occultations	15 sec.	26 sec.
Δh due to time error of .01 sec. of time	5.5 mi.	4.6 mi.
Δh due to angular error of 1 sec. of arc	2.33 mi.	3.33 mi.

Assumptions: 1. Circular orbit around earth; 2. One star occulted per degree of arc.

orbit. Table 2 contains the data for two targets at distances of 200 and 2000 miles above the surface of the earth for the conditions of two occultations separated by 1 degree. Input errors of 0.01 second in time and 1 second of arc have been assumed. The orbit errors are capable of being reduced by additional occultations.

The knowledge that a target is following a ballistic course may be utilized to improve system sensitivity. When operating at low signal-to-noise ratios, a false indication of star occultation may occur. However, if this occultation were stored and compared with future occultations, it could be evaluated as to whether it was false. In effect, this is equivalent to a very powerful scan-to-scan correlation technique. By increasing the computer capacity, operation at lower signal-to-noise levels is feasible.

Limitations

General

Limitations of the star occultation technique stem directly from the nature of light itself. They fall into two categories in accordance with the dual character of light: (1) the wave character of light imposes range limitations; (2) the granular character of light imposes velocity limitations.

Range Limitation

An object passing in front of a star does not cast a true geometric shadow—it forms a diffraction pattern. The smaller the object or the greater the distance to the observer, the larger the diffraction pattern, until finally the object cannot be discerned as occulting a star. Table 3 contains a chart indicating the ranges and object sizes at which this limitation begins to be noticeable.

It should be realized though that the ranges shown

TABLE 3

Diffraction Limitation

Effective Target Diameter	Effective Telescope Diameter	Range for Reduction of Effective Occultations
Feet	*Inches*	*Miles*
10	20	2,400
	100	12,000
100	20	24,000
	100	120,000

$R \propto$ (Effective Telescope Diameter) $\times$ (Effective Target Diameter)*

* Assuming spherical target.

represent a decrease in detection probabilities and not complete absence of information. A bright star will still give evidence of a partial occultation. Of interest is the fact that available equipment will effectively operate right to this limit. Astronomers obtain data by working into the diffraction pattern.

Velocity Limitation

General.—Velocity limitation, the more serious of the two limitations, is due to the granular nature of light. Light from a star travels in small packets of energy called photons. The ability to detect a star is determined by the presence of a certain number of photons per second striking the detecting device. In the illustrations used thus far, 16,000 photons per second are entering the telescope aperture for the dimmest detectable star. Thus, if an object occults a star for about $\frac{1}{16{,}000}$ second, it would be difficult to determine whether the star has been occulted, since in such an interval the chances are about 37 percent that a photon would not have arrived.

In addition, the characteristics of the detector create further difficulties since the detector does not necessarily respond to each photon. The detector is only responsive to certain wavelengths, and then only to a percentage of photons within that wavelength. For example, the efficiency of the eye to sunlight is about 1 percent, which means that, on the average, 100 photons are required to obtain a response from the eye. The image intensifier orthicon has an efficiency of approximately 6 percent.

False Alarm Rate.—Due to the fluctuating photon count, the problem exists of determining whether an occultation or a "false alarm" has occurred. In Appendix I is an outline of the method for determining the average false alarm rate.

Figure 6 contains a plot of average false alarm rate vs. occultation time for 16,000 effective photons per second from the dimmest detectable star. This figure indicates a rapid decrease in the false alarm rate with a very small increase in occultation time. Therefore in order to obtain a reasonable false alarm rate, the time of occultation is generally such that an average of 12

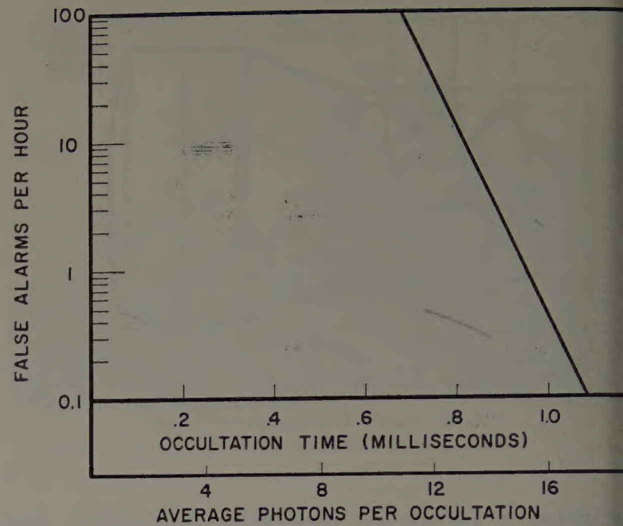

Fig. 6. Average False Alarm Rate vs. Occultation Ti for 16,000 Effective Photons per sec.

to 16 photons normally arrive from the dimm allowable star.

In the preceding illustrations indicating the numb of occultations per degree with various telescope a object sizes, allowances were not made for veloci limitation. Table 4, however, contains a tabulation the velocity at which effective occultation decreas assuming an average false alarm rate of 1.0 occultati per hour per star.

TABLE 4

Velocity Limitation

Detector	Photo-Electron Eff.	Average Effective Photons/Sec	Object Size	Detection Probability Decreases at Velocities of
			Feet	*Miles per hou*
Ideal	1.0	16,000	10	7,000
			100	70,000
Image Intensifier Orthicon	.06	1,000	10	550
			100	5,500
Eye (Equiv.)	.01	160	10	100
			100	1,000

Detection probability.—As a target sweeps across t observer's field of view, normally three occultatio will provide a reasonably accurate determination of path. However, because of the erroneous informati produced by false alarms, four occultations are deem a practical minimum for obtaining reliable and accura data. Hence the problem becomes one of determini the star density required to ensure a high probabili of obtaining at least four occultations during the ti that the target is within the field of view of the te scope. Figure 7 graphically depicts this probability a function of average number of occultations. T average number of occultations required is ten for percent detection probability.

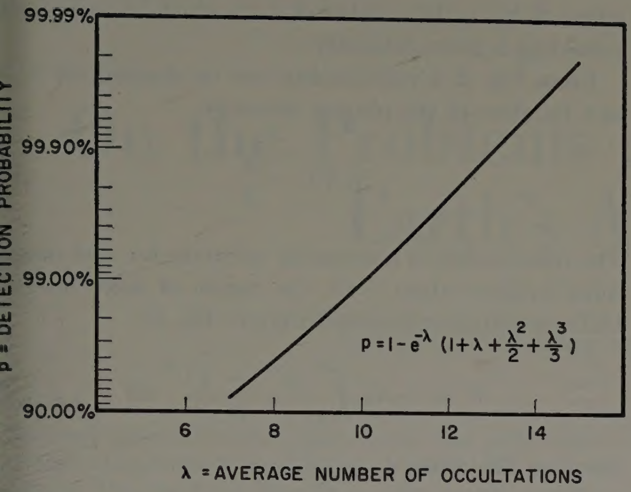

FIG. 7. Probability of Occulting 4 or more Stars

Whether a star is usable depends on the time of ccultation which, in turn, is dependent on the length nd velocity of the target. These factors are shown in heir relation to telescope diameter in the following quations:

$$\text{elescope Diameter} \propto \left(\frac{1}{\text{Occultation Time}} \times \frac{1}{\text{Angular Width of Target}}\right)^{1/2} \quad (1)$$

r,

$$\text{Telescope Diameter} \propto \left(\frac{\text{Velocity}}{\text{Length}} \times \frac{\text{Range}}{\text{Width}}\right)^{1/2} \quad (2)$$

These equations coupled with a knowledge of star ensity and energy enable one to calculate the size of ne telescope required for a given set of target condi-ons. A typical case is shown below:

Target	= 20 feet x 20 feet
Range	= 200 miles
Velocity	= 18,000 mph (Orbit near earth surface)
False Alarm Rate	= 100/sec
Detection Probability	= 99%
Telescope Diameter	= 31 inches
Field of View	= 40° x 40°
Number of Effective Stars	= 360,000

bility to Detect Orbiting Vehicles

To illustrate the potentiality of the star occultation chnique, consider a vehicle in orbit about the earth. quations 3, 4, and 6 contain a few basic relationships hich emphasize the desirable fact that range varies as ne fourth power of the telescope diameter and the urth power of the target diameter. Equation 3 is mply a restatement of an equation previously de-loped; equation 4 is a statement of the relationship that exists between target velocity and distance to the center of the earth; equation 5 is a simplifying assumption; and equation 6 is the result derived from these three parts.

$$(\text{Telescope Diam}) \propto \frac{(\text{Velocity})^{1/2}(\text{Range})^{1/2}}{(\text{Target Diam})} \quad (3)$$

For Target in a Circular Orbit

$$(\text{Velocity}) \propto \frac{1}{(\text{Distance to Earth Center})^{1/2}} \quad (4)$$

For Simplicity, Assume

$$\text{Distance to Earth Center} = \text{Range} \quad (5)$$

Thus, for Photon Limitation

$$(\text{Telescope Diam})^4(\text{Target Diam})^4 \propto (\text{Range}) \quad (6)$$

Detection capability is demonstrated in the tabulations below, in Table 5, which are the results obtained with Eq 6. Also included is the diffraction limited range.

TABLE 5

Detection Capability

Target	Telescope Diameter	Photon Limited Range* for Orbiting Target	Diffraction Limited Range
Feet	*Inches*	*Miles*	*Miles*
100	30	5,000	34,000
	40	16,000	48,000
	60	80,000	68,000
30	100	5,000	34,000
40		16,000	48,000
100		620,000	120,000

* For ease of calculations: 1. Target assumed to be in circular orbit; 2. Distance from target to earth center assumed equal to range.

APPENDIX I

Derivation of the False-alarm Rate

f = false-alarm rate for a particular star

F = average false-alarm rate per star for all stars

N = number of effective photons arriving at the telescope aperture in 1 second from the star under consideration

T = the occultation duration

Δt = the trial time

p = the probability that no photons arrive in the trial time Δt

q = the probability that a photon arrives in the trial time Δt

r = $T/\Delta t$, the number of trials during an entire occultation

u = mean number of trials required to produce a run of no photons of length r

$S(N)$ = total number of stars which produce a photon intensity of at least N at the telescope aperture.

From standard probability theory,*

$$u = \frac{1 - p^r}{qp^r} = \frac{p^{-r} - 1}{1 - p}. \tag{7}$$

Assuming a Poisson distribution for the arrival of photons from a particular star, the probability that no photons arrive during Δt is

$$p = e^{-N\Delta t}. \tag{8}$$

Substituting this distribution and the definitive form of r into Eq. 7 one obtains

$$u = \frac{e^{TN} - 1}{1 - e^{-N\Delta t}}. \tag{9}$$

For small Δt, Eq. 9 may be rewritten as

$$u = \frac{e^{TN} - 1}{N\Delta t}. \tag{10}$$

The false-alarm rate per star is the reciprocal of the mean recurrence time for a run of length r:

$$f = \frac{1}{u\Delta t} = N(e^{TN} - 1)^{-1}. \tag{11}$$

The average false-alarm rate is the summation of the false-alarm rates of all the stars divided by the total number of stars under consideration.

The summation extends from the lowest-intensity star of interest to the highest intensity stars, which for practical purposes can be considered of infinite intensity:

$$F = \frac{\sum_{N_0}^{\infty} f\Delta S}{\sum_{N_0}^{\infty} \Delta S}, \tag{12}$$

where ΔS is the number of stars which have the false-alarm rate f. In the limit,

$$F = \frac{\int_{N_0}^{\infty} fds}{S(N_0)}, \tag{13}$$

where $S(N_0)$ is the number of stars which have intensit[ies] exceeding a given intensity.

From Fig. 2, a relationship can be derived for $S(N$[$)$] as a function of the photon intensity:

$$S(N) = \frac{K}{N} \tag{14}$$

The relationship is reasonably accurate for star magni[-]tudes brighter than +15, the region of most interes[t]. Differentiating and substituting in Eq. 13,

$$F = -N_0 \int_{N_0}^{\infty} \frac{(e^{TN} - 1)^{-1}}{N} dN \tag{15}$$

Let $x = TN$; then

$$F = -N_0 \int_{TN_0}^{\infty} \frac{(e^x - 1)^{-1}}{x} dx \tag{16}$$

For reasonable false-alarm rates, TN_0, the averag[e] number of effective photons blocked during an occulta[-]tion, is rarely less than 10. Therefore,

$$e^x \gg 1, \tag{17}$$

so that Eq. 16 can be closely approximated by

$$F = -N_0 \int_{TN_0}^{\infty} \frac{e^{-x}}{x} dx \tag{18}$$

This can be expanded in an asymptotic series givin[g]

$$F \approx \frac{e^{-TN_0}}{T}. \tag{19}$$

Equation 19 is plotted in Figure 6.

It is interesting to compare the average false-alar[m] rate, Eq. 19, with the false-alarm rate of the dimme[st] star under consideration, Eq. 11,

$$\frac{F(N_0)}{f(N_0)} \approx \frac{1}{TN_0} \tag{20}$$

TN_0 is about 12 to 16 in most of the examples used.

* W. Feller, Probability Theory and Its Applications (John Wiley & Sons, Inc., New York, N. Y.) p. 286.

On the Problems of Re-entry into the Earth's Atmosphere*

Alfred C. Robinson and Algimantas J. Besonis

bstract

Re-entry into the earth's atmosphere has been studied om the standpoints of deceleration, heating, and accuracy impact. This has been done for re-entry speeds consistent ith return from near satellite orbits, and for speeds constent with re-entry from a circumlunar orbit under several nfigurations of lift and constant or variable drag coefficient sumptions. Heating considerations are based only on stagtion point influences. It is shown that deceleration and ak heating rates are not larger than those occurring in llistic missile re-entries. The total heat input, however, is uch larger as the heating occupies a much longer time. It pears that simple, non-lifting re-entry will be feasible from tellite orbits. The lunar re-entry, on the other hand, prents a severe total heat problem and accuracy requirements e such that some lift or other control will probably be quired.

EC I—Introduction

Before studying the re-entry problem, it is well to ate the criteria of a successful re-entry. The mission ing considered here is that of recovering an instruented or manned vehicle after it has been orbiting e earth or gone around the moon. There are two parts this problem: it must reach the surface of the Earth ithout substantial damage to crew or payload; and must be found. The first aspect is concerned with rodynamic heating, deceleration, and dynamic presre; the second with impact point prediction.

Very little will be said about the configuration of the hicles considered. This is a separate field of investigan and an important one. It is assumed that the bodies e generally blunt and are hemispherical in the region the stagnation point. It is further assumed that the agnation point heating is the most severe on the body, d that therefore it is the only point for which the ating needs to be calculated.

Three types of re-entry are considered: (1) no lift, nstant drag coefficient, (2) no lift, variable drag efficient, (3) low lift. All the studies reported herein e concerned with the behavior of the vehicle inside e atmosphere. All simulations and computations vered deal with motion, heating, etc., from "re-entry itude" down to the surface of the earth. Above the entry altitude, the missile motion may be computed sed on vacuum conditions, except in certain special ses, such as lifetime computations.

* Aeronautical Research Laboratory, ARDC, August 58.

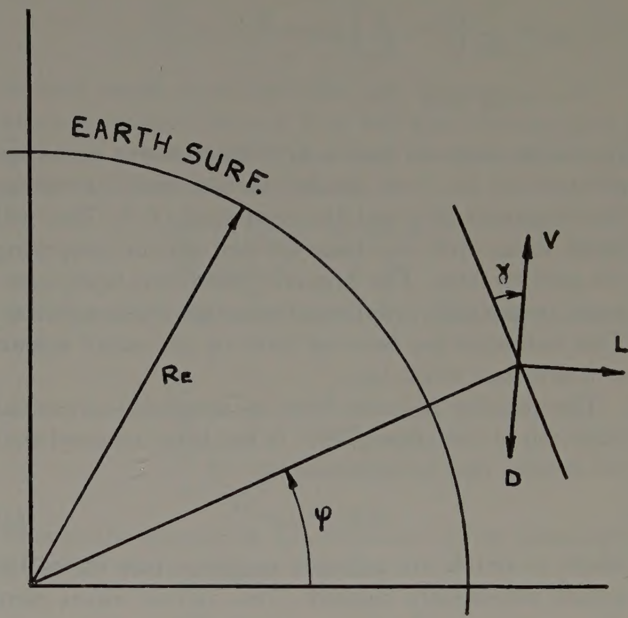

Fig. 1. Coordinate System

In an exploratory study such as this, high accuracy is not required per se. Therefore it was decided to use an analog computer and take advantage of the high speed and flexibility of that equipment. This made necessary one or two points of procedure which could have been omitted otherwise, but it is felt that the utility of the analog computer was such as to justify some slight additional analytical complexity.

SEC II—Development of the Equations

In this section the equations are developed which were used to describe the system mathematically. They fall logically into two divisions: mechanical equations of motion, and the heating equation. They make use of different techniques and disciplines and are largely independent.

A. *The Equations of Motion*

It appears to be adequate for present purposes to consider motion only in a single plane. It would appear that all the important effects can be studied except possibly impact errors. These can be treated as perturbations from the plane. Furthermore, the equations will be developed for a non-rotating earth.

Figure 1 shows the definition of the quantities to be

studied. The equations describing this motion are given below:

$$
\begin{aligned}
\dot{V} &= -q\left(\frac{SC_D}{m}\right) - g\left(1 - \frac{2h}{R_E}\right)\sin\gamma \\
\dot{\gamma} &= -\frac{g}{V}\left(1 - \frac{2h}{R_E}\right)\cos\gamma + \dot{\phi} + \frac{q}{V}\left(\frac{SC_L}{m}\right) \\
\dot{h} &= V\sin\gamma \\
\dot{q} &= \frac{2q}{V}\dot{V} - Kq\dot{h} \\
\dot{\phi} &= \frac{V}{R_E}\left(1 - \frac{h}{R_E}\right)\cos\gamma \\
r &= R_E + h\,,
\end{aligned}
\tag{1}
$$

It will be observed that a first order power series approximation has been applied for the terms involving the reciprocal of r and the reciprocal of r^2. This will result in an error less than 0.4 per cent in computing the gravity force. The dynamic pressure is being computed from a differential equation rather than explicitly. This technique has been set forth by the senior author in a previous work. [4]

The quantity K comes from the assumed exponential variation of the atmosphere. It has been assumed that the density may be expressed by

$$\rho(h) = \rho_0 e^{-Kh} \tag{2}$$

where ρ_0 and K are adjusted to give a best fit for the actual atmosphere desired. The values which were chosen were

$\rho_0 = 2.78 \times 10^{-3}$ slugs/ft^3, and

$K = 4.276 \times 10^{-5}$ ft^{-1}.

This fits the ARDC model atmosphere to about 20 per cent from sea level to 400,000 feet, which is the altitude range of interest. It appears that this is accurate enough for studies of this kind.

B. *Aerodynamic Heating*

Only the region of maximum heating (the stagnation point) is considered since it represents the most critical design area. Blunted bodies of radius R will be considered, since only these types of configurations appear to be practical, because of the high aerodynamic heating rates encountered under re-entry conditions. Since the maximum aerodynamic heating for both re-entry conditions occurs below 300,000 feet altitude, the existence of chemical equilibrium in the stagnation region will be assumed.

Experimental results of Rose and Stark [5], show good agreement with heat transfer rates at the stagnation point of blunt bodies at hypersonic speeds assuming an equilibrium boundary layer, as stated above.

Under these conditions the stagnation point heating rate is given by Fay and Riddell [6].

$$\dot{Q}_a = .94g(\rho_w\mu_w)^{0.1}(\rho_s\mu_s)^{0.4}\{1 + (L_E^{.52} - 1)(\bar{h}_D/\bar{h}_s)\}\{(\bar{h}_s - \bar{h}_w)(du/dx)_s^{0.5}\}$$

assuming a Prandl number of 0.71.

Equation 3 in its present form is rather lengthy analog simulation. Order of magnitude analysis in cates that it can be simplified and reduced to a relati lending itself more readily for the present purp while still retaining the essential parameters influen ing stagnation region heat transfer.

Consider the following approximations

$$(L_E^{0.52} - 1)\frac{\bar{h}_D}{\bar{h}_s} \ll 1$$

$$(\rho\mu)_w^{0.1} \sim (\rho\mu)_s^{0.1}$$

$$h_s - h_w \sim \frac{U_\infty^{\,2}}{2j}.$$

Under these assumptions Eq 3 reduces to

$$Q_a = .94g(\rho\mu)_s^{0.5}\frac{U_\infty^{\,2}}{2j}(du/dx)_s^{0.5}.$$

An approximate solution for the nondimensio velocity gradient at the stagnation point in hyperso flow is given by Ting Yi Li [7] as

$$\frac{2R}{U_\infty}\left(\frac{du}{dx}\right)_s = \frac{1}{k}\left\{\left(\frac{1-k}{1+\bar{K}\delta}\right)^2 - \left(\frac{1-4k}{k}\right)\right\}.$$

Then assuming that a Sutherland type viscosity efficient relation holds

$$\dot{Q}_a = 6.2076 \times 10^{-9}\left[\frac{\rho_\infty}{k}\frac{F(k)}{R}\right]^{0.5} U_\infty^{3.0}.$$

$F(k)$ is shown in [9] as a function of k.

The density ratio k has been computed by Feldm [8] as a function of velocity and altitude up to satell velocities for chemical equilibrium behind the sh wave. It should be noted that the density ratio k at high velocities considered equals the density ra behind the shock wave consistent with the assumpti made by Ting. This equality is well indicated Feldman.

The density ratio k for lunar re-entry bodies (ini velocity of 36,000 ft/sec) can be computed from tab computed by Gilmore [9], for equilibrium composit of air and the normal shock relations in a man similar to the computation of Feldman.

Computations of the parameter $[F(k)/k]^{0.5}$ for configurations considered indicate that the variat of this parameter in the range of high heating rate sufficiently low to justify its considerations as a c stant equal to 3.7; then Equation 9 reduces to

$$\dot{Q}_a = 2.3 \times 10^{-8}\left[\frac{\rho_\infty}{R}\right]^{0.5} U_\infty^{\,3}.$$

It should be noted that the assumption of chem equilibrium for all re-entry conditions will give sligl

wer heating rates for the high drag configurations, it the results should still be within the accuracy of) per cent attainable in experimental verification.

The assumption of viscosity variation with tempera-re according to a Sutherland type relation will give wer viscosity coefficients than predicted by Hansen 0] for chemical equilibrium up to temperatures of 00°K. At higher temperatures a very sudden drop in e ratio of the viscosity coefficient as predicted by ansen to the coefficient considered is observed, but is effect of the variation of the viscosity coefficient ith temperature on the heating rate is weakened by e square root dependence of the heating rate on the scosity coefficient.

. *Approximate Solution*

As an introduction to the method which was used to cast the equations for computer use, it is instructive consider an approximate analytical solution which as presented by Allen and Eggers [1]. The develop-ent which follows is not in any fundamental way fferent from theirs. It differs only in the way solutions e presented and in the use of non-dimensionalizing ctors.

If the missile enters with sufficient steepness into the mosphere, the decelerations will be very large, and ot much distance around the earth will be traversed. nder these conditions, the earth might be considered flat and non-rotating. Equating force along the rela-ve wind axes gives for Eq. 1

$$\dot{V} = -\rho_0 e^{-Kh} V^2 \frac{SC_D}{2m} + g \sin\gamma$$
$$\dot{\gamma} = -\frac{g}{V}\cos\gamma. \tag{11}$$

is also necessary to use the relation $\dot{h} = V\sin\gamma$ to mplete the set of equations. It is assumed that avity is a negligible force and that SC_D/m is constant. oth these assumptions are relatively good at the high itudes and high speeds which are usually of interest. gravity is negligible, the flight path angle will not ange. Negative flight path angles will be of interest we substitute $\gamma = -\theta$ and the equation becomes

$$\frac{dh}{dt} = -V\sin\theta$$
$$\frac{dV}{dt} = -\frac{\rho_0 SC_D}{2m} e^{-Kh} V^2. \tag{12}$$

iminating time between these two equations gives

$$\frac{dV}{V} = \frac{\rho_0 SC_D}{2m\sin\theta} e^{-Kh}\, dh. \tag{13}$$

this point we make a change of variable

$$x = Kh - \ln\left(\frac{C_D S}{m}\right)\frac{\rho_0}{2K\sin\theta}. \tag{14}$$

With this change, Eq 13 becomes

$$\frac{dV}{V} = e^{-x}\, dx \tag{15}$$

which may readily be integrated to give

$$\frac{V}{V_E} = e^{-e^{-x}} = f_1(x). \tag{16}$$

If Eq 14 together with Eq 16 are substituted into the expression for acceleration in Eq 12, it may be shown that

$$\frac{dV}{dt} = -K\sin\theta\, V_E^2 e^{-x} e^{-2e^{-x}}. \tag{17}$$

It may easily be shown that the function $e^{-x}\, e^{-2e^{-x}}$ has a maximum value of $1/2e$ and that this maximum occurs at $x = 0.693147$. Therefore, the maximum value of acceleration is given by

$$\left.\frac{dV}{dt}\right]_{\max} = -\frac{K\sin\theta V_E^2}{2e}. \tag{18}$$

so the ratio of the acceleration to the maximum accelera-tion is

$$\frac{\dfrac{dV}{dt}}{\left.\dfrac{dV}{dt}\right]_{\max}} = 2e^{1-x-2e^{-x}} = f_2(x). \tag{19}$$

This is the second of the functions to be tabulated. From Eq 12 it may be seen that

$$\frac{dh}{dt} = -V\sin\theta = \frac{dx}{K\,dt}. \tag{20}$$

From this, it follows that

$$e^{e^{-x}}\, dx = -KV_E\sin\theta\, dt. \tag{21}$$

In integrating this expression, a question arises as to the definition of zero time. Arbitrarily, the time corre-sponding to maximum deceleration has been selected as the origin of time. The integrand $e^{e^{-x}}dx$ may be transformed by substitutions of $e^{-x} = z$. Using this transformation

$$\int_{x_1}^{x_2} e^{e^{-x}}\, dx = -\int_{e^{-x_1}}^{e^{-x_2}} \frac{e^z}{z}\, dz = KV_E\sin\theta t \tag{22}$$

at the point of maximum deceleration, $e^{-x} = \frac{1}{2}$. There-fore, the integral to be evaluated is

$$\int_{0.5}^{e^{-x}} \frac{e^z}{z}\, dz = KV_E\sin\theta t = \tau \tag{23}$$

where τ is a non-dimensionalized time. Evidently, Eq 23 may be written

$$\tau = \int_{-\infty}^{e^{-x}} \frac{e^z}{z}\, dz - \int_{-\infty}^{0.5} \frac{e^z}{z}\, dz = f_3(x). \tag{24}$$

This is the third of the tabulated functions. This in-tegral has been tabulated by Blanch. [11]

There is another set of equations which is important in this problem, namely those relating to aerodynamic heating. It has been shown by various authors that the aerodynamic heating rate at the stagnation point may be expressed by an equation of the form

$$\dot{Q}_a = \frac{A}{\sqrt{R}} \sqrt{\rho_\infty}\, V^a. \qquad (25)$$

If V is in feet per second, ρ_∞ in slugs per cubic foot and R in feet and $\dot{Q}_a$ in BTU per square foot per second, and $a = 3$, then A is approximately 2.3 times 10^{-8}. It is possible to non-dimensionalize Eq 25 in much the same way as the earlier equations and the result is

$$\dot{Q}_a = \frac{A}{\sqrt{R}} \sqrt{\frac{2K \sin\theta}{\left(\frac{C_D S}{m}\right)}}\, V_E{}^a e^{-x/2} e^{-ae^{-x}} \qquad (26)$$

It may easily be shown that this has a maximum when $x = \ln 2a$ and that this maximum is

$$\dot{Q}_a\big]_m = \frac{A}{\sqrt{R}} \sqrt{\frac{2K \sin\theta}{\left(\frac{C_D S}{m}\right)}}\, V_E{}^a \frac{1}{\sqrt{2ae}} \qquad (27)$$

so that the ratio of the heating rate to the maximum heating rate is given by

$$\frac{\dot{Q}_a}{\dot{Q}_a\big]_m} = \sqrt{2ae}\, e^{-x/2-ae^{-x}} = f_4(a, x). \qquad (28)$$

This is the fourth of the tabulated functions. Equation 26 may be integrated over x to give the total heat input down to any specific value of x. The result is

$$Q_a = -\frac{AV_E^{a-1}}{\sqrt{R}} \sqrt{\frac{2}{K \sin\theta \left(\frac{C_D S}{m}\right)}} \cdot \int_{+\infty}^{x} e^{-x/2-(a-1)e^{-x}}\, dx. \qquad (29)$$

This integral may be transformed by use of the substitution $(a - 1)e^{-x} = u^2$, so that Eq 29 becomes

$$Q_a = \frac{AV_E^{a-1}}{\sqrt{R}} \sqrt{\frac{2}{K \sin\theta \left(\frac{C_D S}{m}\right)}} \cdot \frac{2}{\sqrt{a-1}} \int_0^{\sqrt{a-1}e^{-x/2}} e^{-u^2}\, du \qquad (30)$$

The final value of Q_a is

$$Q_a\big]_m = \frac{AV_E^{a-1}}{\sqrt{R}} \sqrt{\frac{2}{K \sin\theta \left(\frac{C_D S}{m}\right)}} \sqrt{\frac{\pi}{a-1}}. \qquad (31)$$

The ratio of the total heat input to the final value is given by

$$\frac{Q_a}{Q_a\big]_m} = \frac{2}{\sqrt{\pi}} \int_0^{\sqrt{a-1}e^{-x/2}} e^{-u^2}\, du = f_5(a, x) \qquad (32)$$

which is the fifth of the tabulated functions. This integral is simply the probability integral and has been tabulated by numerous authors. To summarize the fi tabulated functions are listed below:

$$f_1(x) = \frac{V}{V_E} = e^{-e^{-x}}$$

$$f_2(x) = \frac{\dot{V}}{\dot{V}_{\max}} = 2e^{1-x-2e^{-x}}$$

$$f_3(x) = \tau = \int_{0.5}^{e^{-x}} \frac{e^z}{z}\, dz.$$

$$f_4(a, x) = \frac{\dot{Q}_a}{\dot{Q}_a\big]_m} = \sqrt{2ae}\, e^{-x/2-ae^{-x}}.$$

$$f_5(a, x) = \frac{Q_a}{Q_a\big]_m} = \frac{2}{\sqrt{\pi}} \int_0^{\sqrt{a-1}e^{-x/2}} e^{-u^2}\, du.$$

$f_1(x)$, $f_2(x)$ and $f_4(x)$ were computed to six-figu accuracy using tables given by Comrie [12] and rounde off to four significant figures. $f_3(x)$ was tabulated usi the nine-figure tables of Blanch. The probabili integral $f_5(x)$ was taken from Peirce [13] though a other standard table of the probability integral wou serve.

TABLE 1

Values of Functions

x	$f_1(x)$	$f_2(x)$	$f_3(x)$	$f_4(3, x)$	$f_5(3, x)$
	0.	0.		0.	0.
−1.0	0660	0643		0019	9990
−0.8	1080	1412		0076	9971
−0.6	1617	2590	+3.8703	0230	9931
−0.4	2250	4104	+2.8226	0562	9854
−0.2	2948	5771	+2.0472	1144	9729
0.0	3679	7368	+1.4409	2011	9545
+0.2	4410	8656	+0.9451	3134	9297
+0.4	5115	9536	+0.5247	4426	8985
+0.6	5776	9955	+0.1573	5766	8617
+0.8	6381	9945	−0.1718	7032	8200
+1.0	6922	9585	−0.4722	8124	7749
+1.2	7399	8965	−0.7515	8979	7276
+1.4	7815	8187	−1.0143	9570	6794
+1.6	8172	7330	−1.2644	9902	6312
+1.8	8476	6457	−1.5046	9999	5839
+2.0	8734	5613	−1.7372	9899	5381
+2.2	8951	4827	−1.9631	9641	4944
+2.4	9133	4114	−2.1844	9266	4531
+2.6	9284	3481	−2.4009	8808	4143
+2.8	9410	2927	−2.6154	8298	3781
+3.0	9514	2450	−2.8266	8109	3446
+3.2	9601	2043	−3.0358	7215	3136
+3.4	9672	1697	−3.2434	6675	2852
+3.6	9730	1406	−3.4495	6150	2591
+3.8	9779	1163	−3.6545	5648	2352
+4.0	9829	0962	−3.8585	5189	2134
+4.2	9851	0791	−4.0619	4728	1935
+4.4	9878	0651	−4.2647	4313	1754
+4.6	9900	0536	−4.4668	3929	1589
+4.8	9918	0440	−4.6687	3574	1440
+5.0	9933	0360	−4.8702	3249	1304
+5.2	9945	0297	−5.0714	2950	1181
+5.4	9955	0243	−5.2734	2678	1069
+5.6	9963	0200	−5.5038	2429	0968
+5.8	9970	0164	−5.6769	2202	0876
+6.0	9975	0134	−5.8771	1996	0793

In order to use this table, it is necessary first to com-
oute the maximum value of each of the functions.

Once these have been computed, it is only necessary o multiply them by the appropriate value of function rom Table 1 in order to get the value of the variable or the associated values of x. It remains, then, to letermine the relationship between x and h. This is given in Eq 14. By this means a complete solution subject to the above named approximations may be ound for any specific re-entry.

). *Normalized Equations*

Consider the following changes of variable:

$$V = V_E v \qquad t = \frac{\tau}{K V_E \sin\theta} \qquad q \overset{\Delta}{=} \frac{K \sin\theta V_E^2}{2e\left(\frac{C_D S}{m}\right)} \bar{q}$$

$$\dot{Q}_a \overset{\Delta}{=} \dot{\bar{Q}}_a \frac{A}{\sqrt{R}} \sqrt{\frac{2K \sin\theta}{\left(\frac{C_D S}{m}\right)}} \frac{V_E^3}{\sqrt{6e}} \qquad (33)$$

$$x = Kh - \ln\left(\frac{C_D S}{m}\right) \frac{\rho_0}{2K \sin\theta}.$$

f these transformations are introduced into the Eq 1 nd normalized Eq 26, the result is

$$\frac{dv}{d\tau} = -\frac{\bar{q}}{2e} - B\left(1 - \frac{2h}{R_E}\right) \sin\gamma$$

$$\frac{d}{d\tau} = -B\left(1 - \frac{2h}{R_E}\right)\frac{\cos\gamma}{v} + \frac{d\phi}{d\tau} + \frac{\bar{q}}{2ev}\left(\frac{C_L}{C_D}\right)$$

$$\frac{dx}{d\tau} = C\, v \sin\gamma \qquad x_0 = 8.601 \qquad (34)$$

$$\frac{d\bar{q}}{d\tau} = \frac{2\bar{q}}{v}\frac{dv}{d\tau} - \bar{q}\frac{dx}{d\tau}; \qquad \frac{d\phi}{d\tau} = Ev\left(1 - \frac{h}{R_E}\right)\cos\gamma$$

$$h = \frac{1}{K}\{x + F\} \qquad \dot{\bar{Q}}_a = \sqrt{3}\sqrt{\bar{q}}\, v^2$$

vhere

$$B = \frac{g}{K V_E^2 \sin\theta} \qquad C = \frac{1}{\sin\theta} \qquad E = \frac{1}{K \sin\theta\, R_E}$$

$$F = \ln\left(\frac{C_D S}{m}\right) \frac{\rho_0}{2K \sin\theta}.$$

'hese are the equations solved on the computer. Changes of variable were based on the maximum values ccurring in the simplified solution of the preceding ection. The maxima which actually occur during re- ntry may differ from those calculated. It should also e understood that the parameters V_E and θ used in the ormalization are not necessarily the actual entry speed nd angle. It is convenient to use values of V_E and θ vhich are near the actual values.

The "re-entry altitude" at which "re-entry angle" defined is that corresponding to $x = 8.601$. From 'able 1, it is seen that, at this point in the approximate olution, about 0.02 per cent of the velocity loss due to

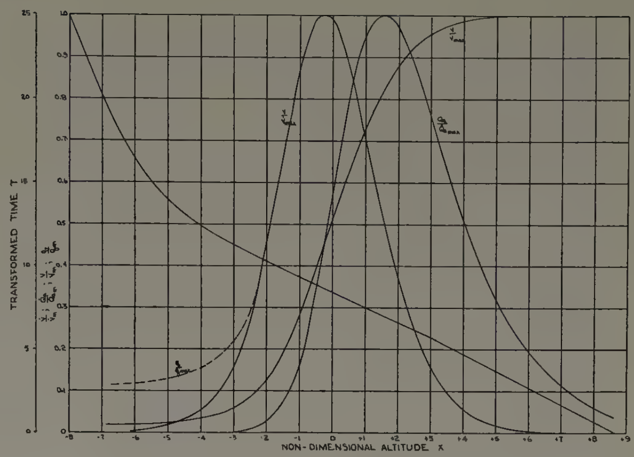

FIG. 2. Normalized Variables vs Altitude

drag has occurred, the heating rate is about 5 per cent of maximum, and about 2 per cent of total heat input has occurred. This was selected as the starting point for all computer runs though it does not correspond to the same altitude in every case. The initial varies from 300,000 feet to 480,000 feet, depending on re-entry speed and angle. The exact value in any particular case may be computed from Equation 14.

SEC III—Re-entry from Satellite Orbits. No Lift, Constant Drag Coefficient

Many different combinations of parameters were studied, and while it might be possible to keep recordings such as Fig. 2 for each case, the resulting volume of data would make intelligent comprehension impossible. Accordingly, for the most part attention was fixed on maxima of the various curves. Figure 3 shows plots of these maxima for the cases studied. Three different re-entry velocities were considered: 25,000, 26,000 and 27,000 ft/sec. Figure 3A shows the peak decelerations, as a function of re-entry angle. Simulator results for the three re-entry speeds are indicated by the solid curves. The dashed curves represent the values predicted by the approximation of section IIC. It may be seen that in all cases the simulator solution approaches the analytical solution as the angle increases. The analytical solutions are all straight lines passing through the origin. At small re-entry angles, the simulator results deviate seriously from the analytical results, as would be expected. However at an angle of 10°, the analytical result gives a fairly good representation. It may be seen that at small re-entry angles, the lower the speed, the higher the deceleration. At higher re-entry angles, this trend is reversed.

It is also necessary to know the range over the earth which the missile traverses between re-entry and impact. Equally important is the sensitivity in range to errors in the re-entry conditions. Figure 4 shows the range as a function of re-entry angle for each of the three speeds studied. The range increases rapidly for small re-entry angle. The curves shown are independent

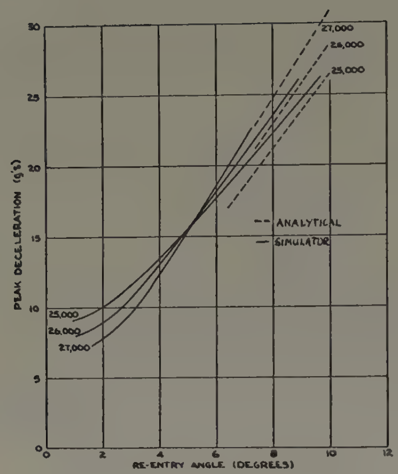

FIG. 3a. Peak Deceleration vs Re-entry Angle.

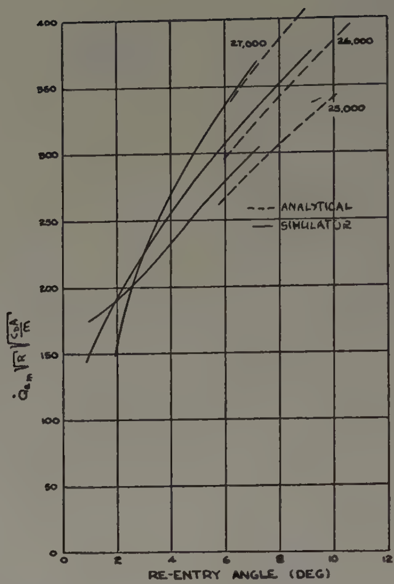

FIG. 3b. Heating Rate Parameter vs Re-entry Angle.

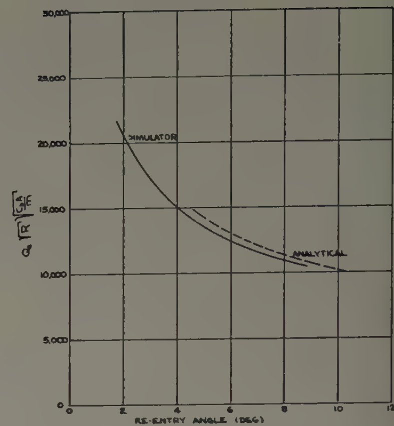

FIG. 3c. Total Heat Parameter vs Re-entry Angle.

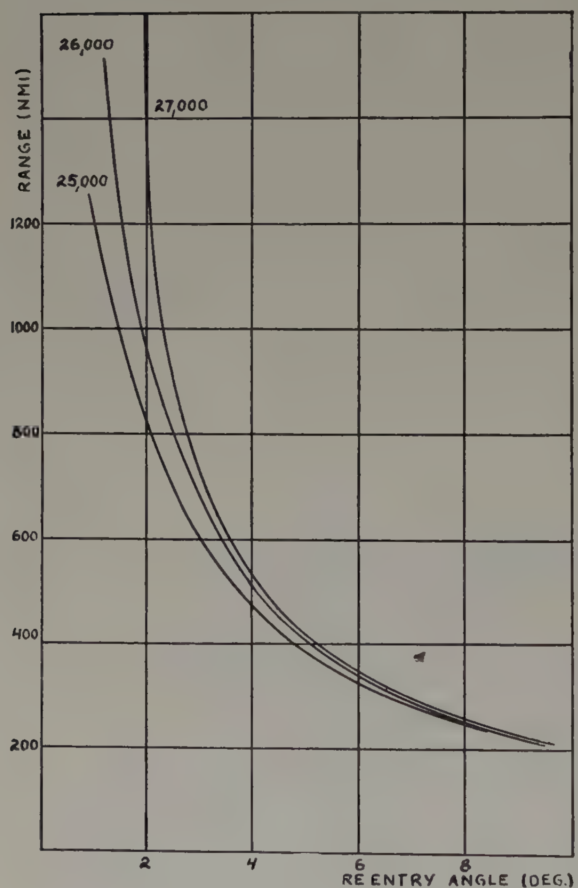

FIG. 4. Range from Re-entry

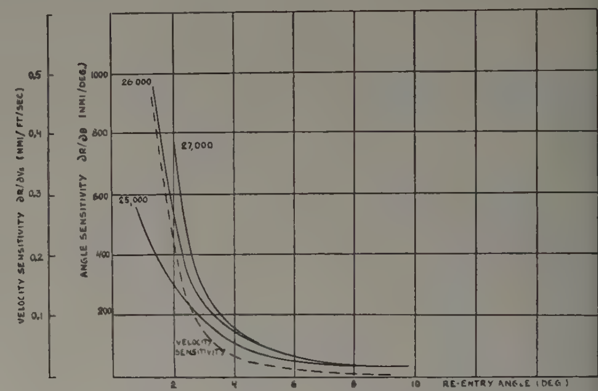

FIG. 5. Range Sensitivity to Re-entry Speed + Angl
Error.

of C_DA/m , but it should be recalled that this is the range from re-entry until impact, and that re-entry altitude depends strongly on C_DA/m. In determining the impact point, this should be kept in mind.

Possibly more important is the sensitivity of this range to various errors. Some of these are shown in Fig. 5. The sensitivity to re-entry angle error is show for each of the three speeds studied, and the sensitiv ity to re-entry speed error is shown for 26,000 ft/se only (dashed curve). Observe that at about 3°, all th curves start increasing rapidly for smaller angles. I possible, the re-entry angle should be kept larger tha 3°, to improve impact accuracy.

These sensitivities might be made more meaningfu by taking an example. It is assumed that the re-entr angle uncertainty will be 0.1°, the re-entry velocit uncertainty 20 ft/sec, and that the density uncertaint is 30 per cent at all altitudes of interest. If thes assumptions are used for the errors, the results o Fig. 6 are obtained. The three error contributions ar shown as a function of re-entry angle, and also th combined error. Again it may be seen that from th accuracy standpoint, re-entry angles smaller tha about 3° are very undesirable. At small re-entr angles, the angle uncertainty is the predominant erro At steeper angles, the density uncertainty become dominant. The velocity error contribution is negligibl

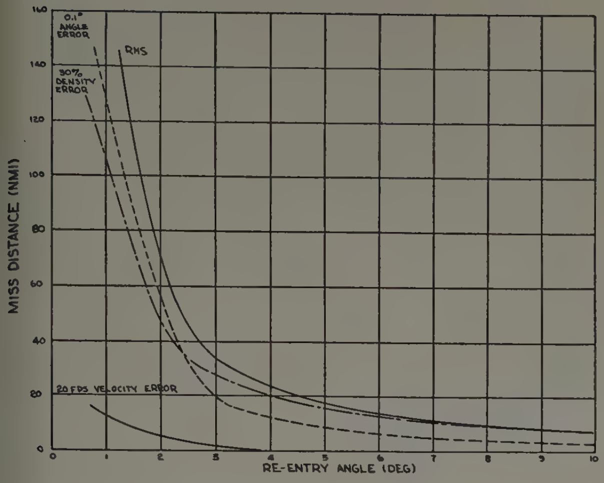

FIG. 6. Miss Distance for Satellite Re-entry

t all angles. The nominal re-entry speed assumed for ig. 6 was 26,000 ft/sec.

All the foregoing data are summarized on Fig. 7. For re-entry vehicle of this type, there are only a few hoices open to the designer. The re-entry speed is xed by the type of orbit from which the vehicle is escending. There remain only the re-entry angle, the rag-mass parameter and the stagnation point radius f curvature to choose. In Fig. 7, the re-entry angle is lotted against the product of R and C_DA/m. Every pecific set of choices of the three variable parameters, hen, will correspond to a point in the plane of Fig. 7. Vhile re-entry angle is the primary ordinate, peak eceleration and impact uncertainty are plotted as dditional ordinates inasmuch as they are single-valued nctions of re-entry angle. In this, the re-entry speed as been assumed to be 26,000 ft/sec, which is close the re-entry speed for the lowest satellite orbits.

We are now in a position to discuss the problem of -entering the earth's atmosphere with this type of hicle. The heating problem is the most complicated, it will be considered first. Obviously the most desir- ble heating situation is one where all the heat which ters the body may be re-radiated. This would require at peak heating rates be held below about 20 BTU/ ²/sec, and this in turn would require that $R\ C_DA/m$ on the order of 200 even for small re-entry angles. a 5 ft radius of curvature is used, C_DA/m would ve to be 40, which means a very light, high-drag ructure indeed, less than 1 pound per square foot of uivalent drag area. As was mentioned earlier, the tal heat input curve for this case is of little interest, cause all the heat is re-radiated.

A more typical blunt configuration would have a A/m on the order of 0.5. Again, taking a five foot dius of curvature, the abscissa of Fig. 7 would be , and it may be seen that the heating rate is some- hat over 100 BTU/ft²/sec even at low re-entry angles. would appear, then, that from the heating rate ndpoint, $R\ C_DA/m$ is going to have to be greater

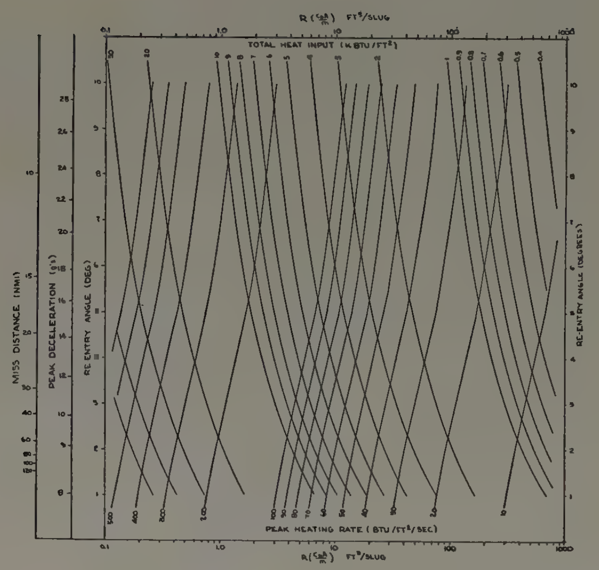

FIG. 7. Design Parameter Diagram, Satellite Re-entry

than 2.5, and the larger the better. If it could be made as large as 200, this would eliminate the need for special heat protection devices.

The peak deceleration starts at a little less than 8 g's at shallow angles, and increases more or less linearly with angle to nearly 30 g's at 10°. For manned flights, the maximum allowable deceleration probably lies somewhere between 10 and 12 g's for the time durations involved. This means that the steepest allowable angle would not be much over 3°.

Impact uncertainty follows the opposite trend. Impact becomes more accurate as re-entry angle is increased. For the manned case, observe that 10 g's peak deceleration corresponds to an impact uncertainty of 40 miles under the assumptions used. It should be emphasized that this 40 miles does not represent the total error. It represents only the error which results from uncertainties in re-entry angle, re-entry speed and atmospheric density uncertainties. There are other uncertainties to be considered, principally the point on the trajectory at which the vehicle crosses the re-entry altitude. This is determined by what happens outside the atmosphere, and is thus beyond the scope of study. This will probably be the largest single source of error.

We see, then, two opposing tendencies: to get accuracy the re-entry angle must be steep, to keep down the peak deceleration the re-entry angle must be shallow. Just how the compromise is to be made depends on the mission of the vehicle.

SEC IV—Re-entry from Satellite Orbit. No Lift, Variable Drag Coefficient

One method which has been proposed for alleviating the re-entry problem is that of varying the drag during the descent. It was indicated in the preceding section that so long as the drag was constant during the run,

the peak deceleration was the same, regardless of what the drag was. Heating rate and dynamic pressure did, of course, depend on $C_D A/m$. If the drag is changed during the re-entry, however, this is no longer the case. It is possible to achieve some reduction in peak deceleration. The purpose of this section is to show how much the deceleration may be reduced, and to investigate the effect on other parameters.

Assume that the vehicle has a means of varying the drag. Let us define the maximum drag by $C_D A/m$, and the actual drag by $(C_D A/m)\epsilon$, where ϵ is a variable factor which lies on the range $0 < \epsilon \leqq 1$. The velocity equation for the flat, non-rotating earth with gravity neglected would be, then,

$$\frac{dV}{dt} = -q\left(\frac{C_D A}{m}\right)\epsilon. \qquad (34)$$

Again using the exponential atmosphere,

$$\frac{dV}{dt} = -\frac{\rho_0}{2} V^2 \left(\frac{C_D A}{m}\right) \epsilon e^{-Kh}. \qquad (35)$$

If we now apply the transformations as before:

$$V = V_E v, \qquad x = Kh - \ln\left(\frac{C_D S}{m}\right)\frac{\rho_0}{2K\sin\theta}, \qquad (36)$$
$$t\, K V_E \sin\phi = \tau$$

then Eq 35 becomes

$$\frac{dv}{d\tau} = -v^2 \epsilon e^{-x}. \qquad (37)$$

The optimum way to make use of variable drag would be to start the re-entry with the drag a maximum ($\epsilon = 1$). It would be maintained at this value (in order to keep the heating down) until the deceleration has reached the maximum desired value. Then ϵ is varied so as to keep the deceleration at this desired maximum. It is this portion of the process which must be considered now. Generally speaking, if the deceleration is to be held constant as the altitude decreases, then,

$$\frac{d}{dx}(v^2 \epsilon e^{-x}) = 0 = -v\epsilon + v\frac{d\epsilon}{dx} + 2\frac{dv}{dx}\epsilon. \qquad (38)$$

It may easily be shown that in this approximate problem,

$$\frac{dv}{dx} = v\epsilon e^{-x}. \qquad (39)$$

Putting this fact into Eq 38 gives

$$\frac{d\epsilon}{dx} = \epsilon - 2\epsilon^2 e^{-x} \qquad (40)$$

which may be combined with Eq 39 to give

$$\frac{d\epsilon}{\epsilon} = dx - 2\frac{dv}{v}. \qquad (41)$$

This may be integrated directly to give

$$\ln\epsilon = x - 2\ln v + \text{Const.} \qquad (42)$$

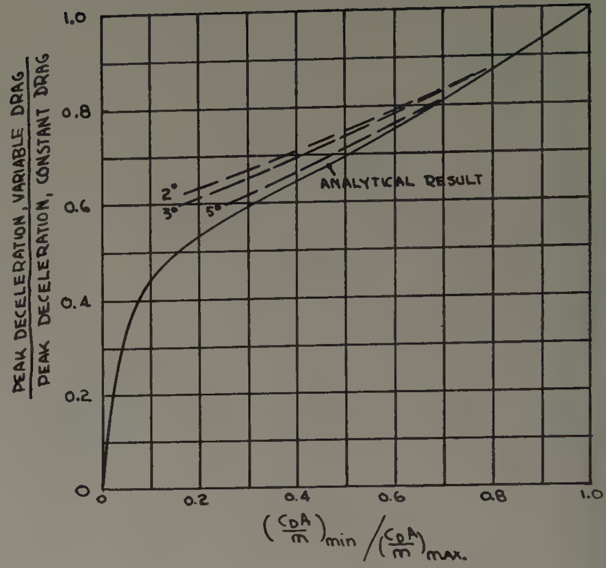

FIG. 8. Effect of Drag Variation

It is now necessary to apply the initial conditions Recall that the above differential equations describ the portion of the trajectory where the deceleration i being held constant. The initial conditions for this ar then, those of the point of the trajectory at which i was decided to begin holding the deceleration constant Assume this occurs as an x of x_0, and a v of v_0, then

$$\epsilon = \frac{e^{(x-x_0)}}{\left(\frac{v}{v_0}\right)^2} \qquad (43)$$

Now, putting this value of ϵ into Eq 39,

$$\frac{dv}{dx} = v\frac{e^{x-x_0}}{\left(\frac{v}{v_0}\right)^2} e^{-x} = \frac{v_0^2}{v} e^{-x_0}$$

$$v\, dv = v_0^2 e^{-x_0}\, dx. \qquad (44)$$

Integrating this equation, and applying the initia conditions, gives the results that

$$\frac{v^2}{v_0^2} = 1 + 2e^{-x_0}(x - x_0). \qquad (45)$$

Combining this with Eq 43 gives

$$\epsilon = \frac{e^{x-x_0}}{1 + 2e^{-x_0}(x - x_0)}. \qquad (46)$$

By differentiating this expression with respect to x an setting the derivative equal to zero, the minimum valu of ϵ may be obtained. It is

$$\epsilon_{\min} = \frac{e\left(1 - \frac{e^{x_0}}{2}\right)}{2e^{-x_0}}. \qquad (47)$$

This may easily be computed as a function of x_0 From Table 1 it may be determined what the decelera tion is at each value of x_0. From a cross-plot of th

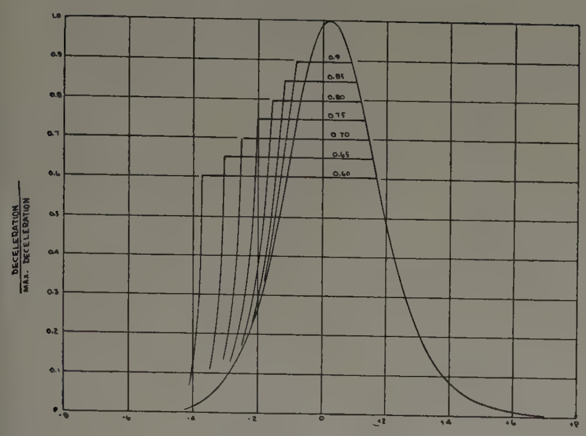

Fig. 9a. Normalized Deceleration vs Normalized Altitude

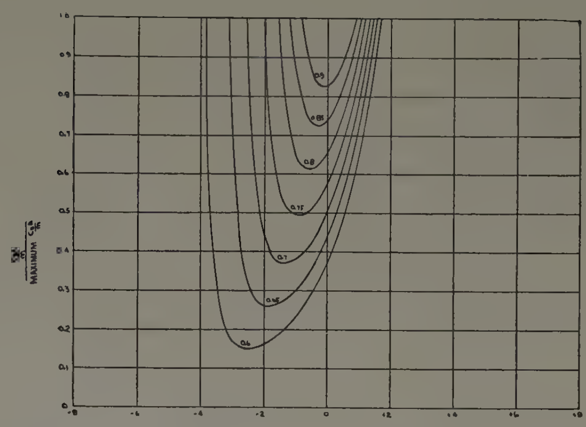

Fig. 9b. Drag Variation vs Normalized Altitude

two, the ϵ_{min} corresponding to each deceleration reduction may be shown. This is given in Fig. 8, as the solid curve.

Figure 9A is a plot of normalized deceleration as a function of altitude, and Fig. 9B is a plot of ϵ as a function of altitude. The deceleration reductions as taken from curves like these have been plotted along with the analytical result in Fig. 8. Three cases were studied, 2°, 3° and 5° re-entry angles. It may be seen that the 5° case agreed with the analytical result the best because, as mentioned earlier, the approximation is better for this case. The other angles disagree somewhat more.

It may be seen from Fig. 8 that it is a relatively easy matter to reduce the peak deceleration by 10, 20 or 30 per cent. Any more than this begins to come hard, however. In order to get a 50 per cent reduction, it would take a rather ambitious drag varying device, something more than 10 to 1. The peak heating rate is unaffected by this drag variation. This is because at least for all the cases studied here, the peak heating had occurred before the drag started to vary. There is some additional heating at lower altitudes, and the total heat will be somewhat higher, but this is not really appreciable. The impact prediction accuracy is not significantly affected.

Various simplifications of this scheme suggest themselves. The first is that of not increasing drag again after it has passed its minimum. The deceleration would start falling immediately after the minimum was passed, and there would be some additional heating at lower altitudes after the maximum had passed, but there would be no great difference, and the primary objective of keeping the deceleration below the prescribed maximum would be attained.

Another possibility is that of a sudden stepwise reduction in drag rather than the gradual, programmed reduction shown in Fig. 9. This was investigated and found to be incapable of reducing the peak deceleration. The deceleration dropped immediately, of course, when the drag was reduced, but later it built up again to higher values, so that it made little or no reduction in the peak deceleration.

In summary, then, it may be said that drag variation offers a possibility of modest reductions in peak deceleration without significant penalty in any other area except for the additional complexity of the drag-varying device. If sizeable reductions in deceleration are desired, however, some other device will have to be found.

SEC V—Lifting Re-entry from Satellite Orbits

It has been proposed to use lift to alleviate various re-entry problems and, in fact, it shows real advantages. Assume that we apply a constant C_L/C_D throughout the re-entry. Figures 10A, B and C show the effect of this lift on peak deceleration, peak heating rate and total heat input, respectively. Results are shown for each of two re-entry angles: 2 degrees and 5 degrees. The reduction in deceleration is approximately the factor 5. The improvement in peak heating rate is not so remarkable, being slightly less than the factor 2. It may be seen that the 5 degree re-entry case is less affected by the lift. This is because, with the steeper re-entry angle, the lift has less time to curve the flight path before peak heating and peak deceleration occur. It might be assumed that even better results could be obtained with shallower re-entry angle.

So far, the use of lift appears to be quite attractive, but its effect on impact accuracy is somewhat more troublesome. Possibly Fig. 11 will give some idea of the nature of the difficulty. It may be seen that as the lift goes up, more and more "skips" take place. Now these skips are somewhat difficult to control. Once the lift has been applied, and the vehicle starts up, it goes into a pure ballistic phase, and it is not possible to control it again until it comes back down into the denser atmosphere. Thus all points between the point it leaves the dense atmosphere and the point it returns are inaccessible to the missile as impact points. The length of these skips is rather critically dependent on

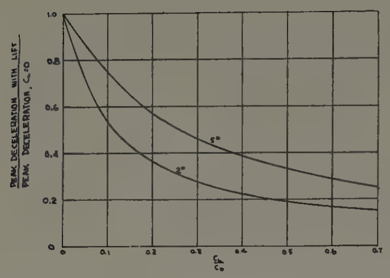

FIG. 10a. Effect of Lift on Peak Deceleration.

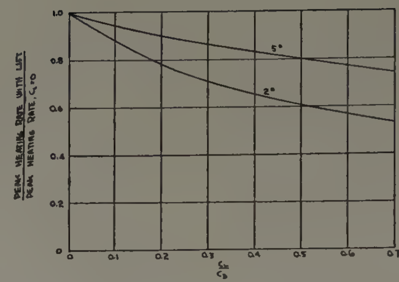

FIG. 10b. Effect of Lift on Peak Heating Rate.

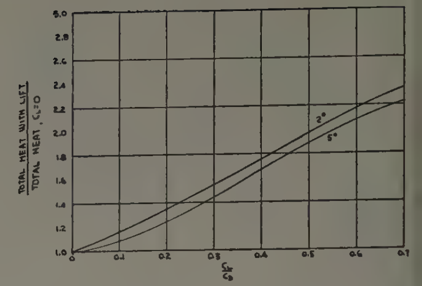

FIG. 10c. Effect of Lift on Total Peak.

the amount of lift applied. On all the trajectories, a point is finally reached where the missile has lost most of its initial speed, and it goes into a nearly vertical fall, at its terminal velocity. This is the point which must be controlled, because relatively little control is available thereafter. Let us say that h_1 is the altitude at which the vehicle loses all its forward speed (aside from that which might be supplied by lift), and call ΔR the amount by which the impact point may be changed by lift. It may be easily shown that

$$\frac{\Delta R}{h_1} = \frac{C_L}{C_D}$$

In no practical case will h_1 be greater than about 180,000 feet. Assuming C_L/C_D of unity would mean that the range could be changed by 180,000 feet in either direction, or about 30 NMI, hardly enough to wipe out the effect of some erroneous skips earlier in the trajectory. In order to use lift to control the impact point, it appears necessary to use a rather elaborate tracking and computer system on the ground and to transmit commands to the missile from time to time during the re-entry. This is a complication which should be avoided if there is any other way to solve the heating and deceleration problems.

In Fig. 11, the open circles indicate the point on each trajectory where maximum deceleration occurs, and the crossed circles indicate that point where maximum heating occurs. Observe that on all the trajectories, the maximum heating occurs early, not long after the lift has begun to separate the paths. The maximum deceleration, however, occurs just before the final plunge into the dense atmosphere. This further illustrates the need to use the lift for deceleration reduction until late in the trajectory, and only then is it free for use in impact control.

A somewhat different situation exists for the steeper re-entry angle as is shown in Fig. 11. Here, both the peak heating and deceleration occur early in the trajectory, even before the first skip. The impact accuracy is much better at the steeper angle, but, on the other hand, with the steeper angle, lift does not offer so much improvement in peak deceleration and heating rate.

In summation, then, it appears that from the standpoints of deceleration and heating rate, lift is very attractive. It raises such problems in impact control, however, that it should be used only if simpler schemes prove unworkable.

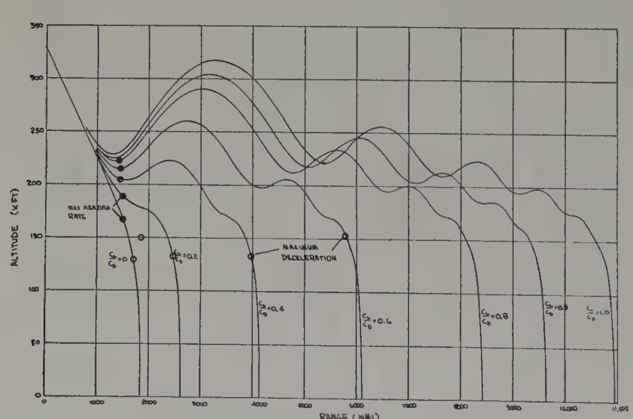

FIG. 11. Lifting Trajectories

SEC VI—Re-entry from Lunar Orbits. No Lift, Constant Drag Coefficient

As the next step in the study, it was decided to proceed to a higher-speed re-entry, consistent with a circumlunar orbit. Only the concept of entering the atmosphere on the first pass was considered in any detail. The intent of the present study is to outline the problems of entering directly. That is to say that once the vehicle enters the atmosphere, it stays in until impact at the surface.

Only one re-entry speed was studied in this case, that of 36,000 ft/sec. Figure 12 shows the characteristics of re-entry at this speed. Figure 12A is the peak deceleration as a function of re-entry angle. This curve has a minimum near 5°, and the curve does not go below 4.8 degrees or so. The reason for these things may be gleaned from Fig. 13. This is a trajectory plot, very similar to that of Fig. 11. For the steeper re-entry angles, the trajectory proceeds more or less directly into the denser atmosphere—as might be expected. At shallower angles, however, the behavior is different. Consider, for instance, the 5° trajectory. The flight path angle decreases after re-entry starts.

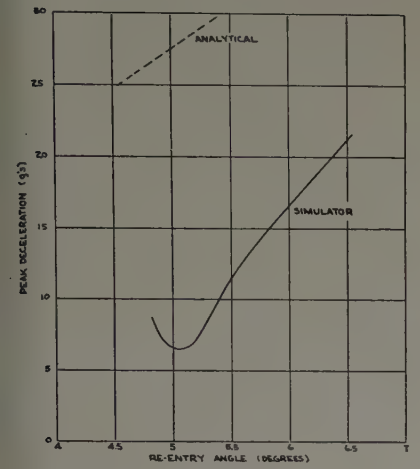

Fig. 12a. Peak Deceleration vs Re-en-
try Angle for Re-entry Speed of 36,000
ft/sec.

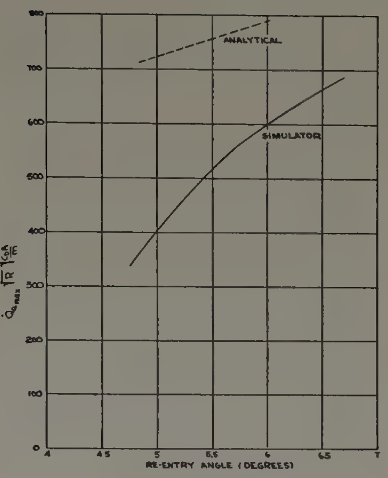

Fig. 12b. Heating Rate Parameter vs Re-entry Angle, for Re-entry Speed of 36,000 ft/sec.

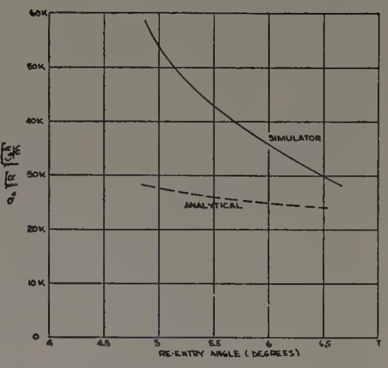

Fig. 12c. Total Heat Parameter vs Re-entry Angle.

until it finally reaches zero, and the vehicle is moving along the local horizontal. Because of the considerable drag existing at this altitude, it finally falls below the satellite speed and starts dropping into the denser regions. It is during this final plunge that the maximum deceleration occurs, though the maximum heating occurred shortly after re-entry. Because of the high vehicle velocity, there is a strong tendency for the vehicle to "graze" the atmosphere, and leave again. This is exactly what happens if the re-entry angle is much less than 5°. The 4°50′ case does in fact leave the atmosphere again, as shown in Fig. 13. For reference, the trajectory for a 5 degree re-entry angle is shown when the effect of atmosphere is deleted. The point of each trajectory where maximum deceleration occurs is indicated by the open circle, and the point where maximum heating rate occurs is indicated by the crossed circle.

Figure 12 shows also the values which would be predicted by the simplified analytical method of Sec. IIC. It may be seen that in all these cases, the analytical solution is in error by something like the factor 2. This is probably due primarily to the fact that the earth cannot be considered flat for these trajectories, and this was one of the assumptions in the analytical development. The agreement between simulator and analytical results was relatively good for satellite re-entry but it is quite poor for lunar ones.

Figure 12B shows the peak heating rate. There is no minimum on this curve because peak heating always occurs early in the trajectory before curvature of the earth or anything else has had much effect. Figure 12C shows the total heat input, and it is what would be expected from Fig. 12B.

Just as in the satellite case, the next consideration is that of uncertainty in the impact point. Range versus re-entry angle for 36,000 ft/sec re-entry speed is shown in Fig. 14. Figure 15 shows the sensitivities, and Fig. 16 the errors which would result, using the same uncertainties as in the satellite case: 30 per cent density uncertainty, 0.1° angle error, 20 fps velocity error. The impact uncertainties run considerably higher here than for satellites.

All these considerations are summarized in Fig. 17, which is analogous to Fig. 7, and is used in just the same way. In fact it is quite interesting to compare the two. First of all, it may be seen that the lunar heating curves are shifted to the right by about the factor 5. This means that to get the same heating, for

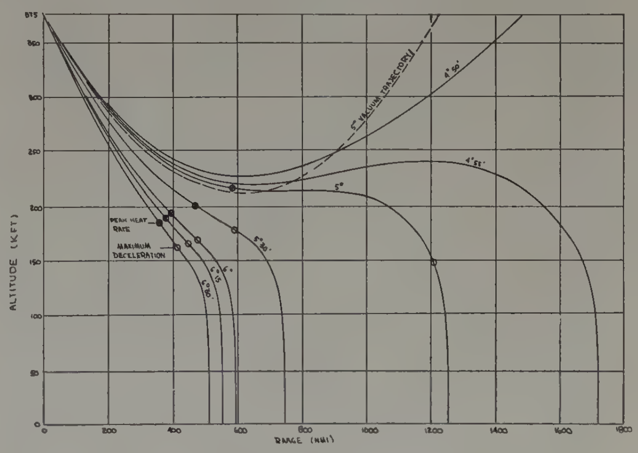

Fig. 13. Lunar Re-entry Trajectory Plots

instance, the lunar RC_DA/m must be about five times greater than the one for satellite re-entry. Putting it the other way around, if the same RC_DA/m is used in both cases, the lunar heating rate will be about $\sqrt{5} = 2.2$ times greater. Of course this depends on the re-entry angle used in the two cases, but it is indicative of the difference. It is interesting that the peak deceleration for the lunar case may actually be somewhat less than the best obtainable in satellite re-entry. Possibly the most significant difference between the two cases

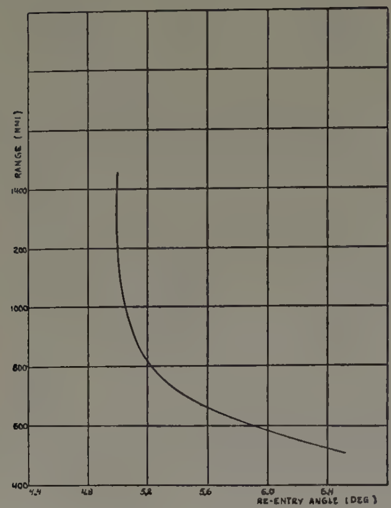

FIG. 14. Range vs Re-entry Angle for Re-entry Speed of 36,000 ft/sec.

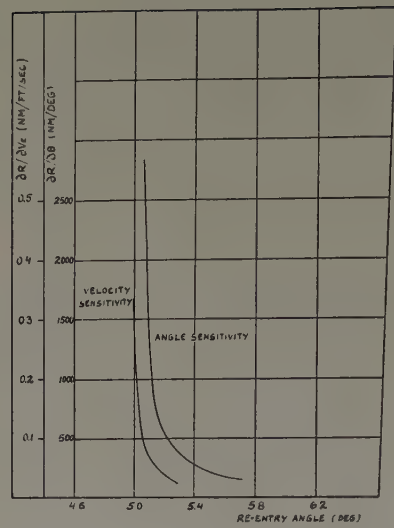

FIG. 15. Range Sensitivities.

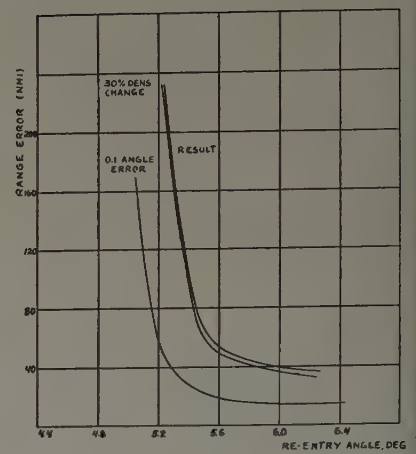

FIG. 16. Range Error Contribution.

is in impact point uncertainty. The lunar ones are much higher. Assume for instance, that we wish to limit the decelerations to 10 g's in both cases. The satellite uncertainty corresponding to this is about 40 NMI, while for lunar re-entry, it is more like 100 NMI. In the latter case the uncertainties are such as to cast doubt on the feasibility of a non-lifting re-entry.

SEC VII—Re-entry from Lunar Orbits. Low Lift, Variable Drag Coefficient

It is possible to use variable drag to decrease the peak decelerations in lunar re-entries, just as in the satellite cases. The same program may be followed, and with much the same result. The reduction in peak deceleration as a function of ϵ, the drag-variability factor falls exactly on top of the 2° curve of Fig. 8. It does not affect peak heating rates, increases total heating slightly, and does not affect impact accuracy.

Lift, in this case is not nearly so effective as in satellite re-entries. It was found that if lift is applied early in the trajectory, in the region of maximum heating and maximum deceleration, then it is not possible to apply more than C_L/C_D of more than 0.1 or 0.2 without causing the vehicle to leave the atmosphere altogether. Applying lift later in the trajectory, of course does not decrease the heating or deceleration, though it provides a means of changing the impact point by a considerable amount. Again, the question of accuracy in controlling C_L/C_D comes into play, however. The accuracy requirements are about the same as those given earlier for the satellite case.

SEC VIII—Results and Conclusions

First of all, it is of interest to present a comparison of the lunar and satellite re-entry problems with each other, and with the more familiar ballistic missile re-entry problem. Figure 18 gives some aspects of thi comparison. In all three figures, the re-entry angle i plotted as the abscissa and a different scale is use for the ballistic missile parameters from that used fo satellite and lunar curves. Figure 18A shows the peal deceleration comparison. For larger angles, more tha 100 g's of deceleration is possible. Satellite and luna decelerations fall in the same range, from 8 to 20 g's and both are well below the corresponding figures fo ballistic missiles. From this standpoint, the satellit and lunar re-entries are easier, and this is principall because of the much shallower re-entry angles. Figur

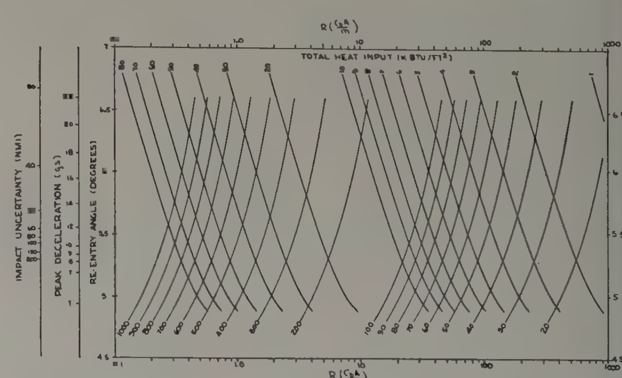

FIG. 17. Design Parameter Diagram, Lunar Re-entry

18B shows the peak heating rate comparison. Her both lunar and satellite values lie above those for th IRBM and below those for the ICBM, and the luna values run considerably higher than the satellite one It should be kept in mind that these comparisons a sume the same values of R and C_DA/m for all the classe of vehicles. This may or may not be the case, but th assumption seems to provide the only meaningf basis for comparison.

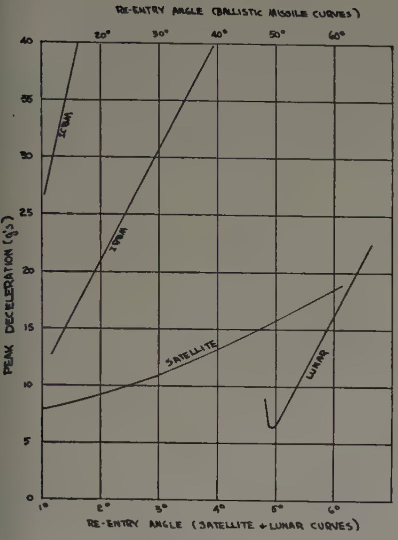

FIG. 18a. Comparison of Peak Decelerations.

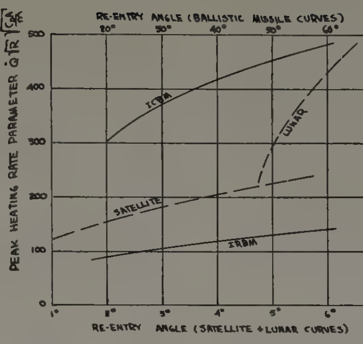

FIG. 18b. Comparison of Peak Heating Rates.

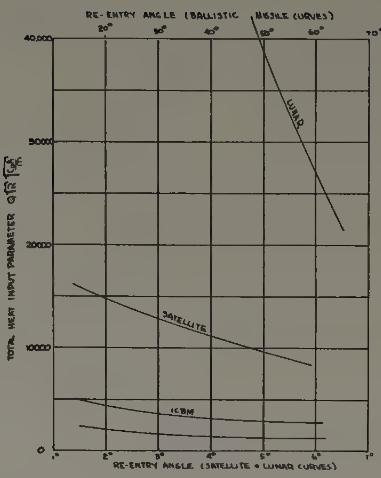

FIG. 18c. Comparison of Total Heat Inputs.

Figure 18C shows the comparison of total heat input, ıd it is here that differences are most marked, and ıe of the major difficulties in satellite and lunar -entry is indicated. The satellite figures run three mes higher than the ballistic missile ones, and lunar -entry some five times higher. As explained earlier, ıis is total aerodynamic heat input, and says nothing ɔout how much is re-radiated. In the steeper angle ses, little is re-radiated, though for shallower angles, -radiation may be an appreciable amount of the hole. In fact if C_DA/m is high enough, all the inlent heat may be re-radiated.

In regard to impact accuracy, of course, ballistic issiles are far superior to the other vehicles. The ain reason is the much steeper re-entry angles used.

Satellite Re-entry Discussion

The simplest system for re-entry is a non-lifting, ustant-drag vehicle, which follows a simple ballistic th. Let us consider the three areas of major concern: celeration, heating and impact error. The peak deceletion can be held to 8 g's with large impact errors, to g's with more reasonable impact errors. Impact curacy may be disposed of by saying that it appears ssible to achieve accuracy sufficient that proper ound installations, suitably alerted, could find the hicle. It does not seem that it will ever be possible th this simple system to deliver the vehicle with curacies sufficient for warhead delivery. If this is be done, some additional control must be provided. ore will be said about this presently.

Heating is probably the most serious problem. In der to avoid ablation or heat-sinks, it would appear cessary to keep RC_DA/m above about 150. This ɔuld mean, for instance a 5 ft radius of curvature and C_DA/m of 30. If excessive ablation rates are to be oided, RC_DA/m must be kept above about 4. With a 5 ft radius of curvature, this would mean a C_DA/m of 0.8. If a heat-sink is to be used, it would have to be large compared to what is used in ballistic missiles, because of the much larger total heat input. BTU/ft^2 of 5000 to 15,000 would be possible for reasonable designs. Study of the heat protection question itself is beyond the scope of the present work. The only intent here is to show the nature of the problem.

Let us now consider possible improvements in accuracy. In a satellite recovery, the main point at issue is the predictability of the impact point. Since the satellite is presumably subject to commands at any point of the orbit, the point at which the recovery is initiated may be easily controlled by the designer. The requirement, then, is to predict how far from this initiation point impact will take place. This is in contrast with the lunar case, where there is no flexibility whatever in the point at which recovery is initiated, and it may be desirable to vary the length of the re-entry trajectory over a wide range. To return to the satellite case, since predictability is the point, and not wide-range control, any mechanism which can eliminate the 100 or 200 *NMI* of error which would normally exist, will be adequate. From Fig. 6 it may be seen that the principal source of error is uncertainty in the atmospheric density. Next comes re-entry angle errors. If really precise impact point control is desired, some way will have to be found for overcoming both these error sources. It would appear that drag variation might do it. The range could be changed by 200 miles or so by changing the drag during descent. This would have to be done with some care to avoid heating and deceleration problems. This area requires further work. In principle, lift could be used to do the same job, but it appears, at least on the surface, that this would be difficult to accomplish, because lift is so difficult to measure. This too, must be studied further.

B. *Lunar Re-entry Discussion*

In this case, deceleration does not appear to be a major problem. It is possible to get decelerations even lower than those for satellites, though at a severe penalty in impact accuracy.

Heat protection is critical, and now so is impact accuracy. In this case there is little that can be done to improve the heating situation except to abandon the idea of re-entry on the first pass. Lift or drag variations seem to offer little improvement. To dissipate all heat by radiation, it will be necessary to keep RC_DA/m above 600 or so. To avoid excessive ablation rates, it would have to be above 25. Even assuming a 10 ft radius of curvature, this would mean C_DA/m's of 60 and 2.5 respectively. The first would appear to be out of the question.

As for impact accuracy, the simple system is marginal at best, and this is leaving aside the not inconsiderable problem of guiding the missile to satisfactory re-entry conditions. From then until impact, the errors developed are serious, and it seems likely that a simple ballistic system will be unfeasible. This is all from the standpoint of predictability alone. It seems quite desirable, and in fact almost a necessity to be able to vary the re-entry trajectory over rather wide limits. If this is not done, the impact point will be determined by the orientation the earth happens to have when the vehicle approaches. While this could be predicted, and accounted for at launch, some flexibility is desirable. There will be various other factors to be considered in selecting a desirable launch time, and it may not be possible to satisfy all requirements simultaneously. There are two obvious ways of supplying this flexibility. One is the use of "braking ellipses" to slow the vehicle down in several passes into the atmosphere, until a more or less circular orbit is achieved, from which final recovery may be initiated. The other method would be to enter on the first pass, but to supply lift or other control after the vehicle had fallen below satellite speed. Further study will be required, but based on present evidence, it is felt that the second alternative is the more preferable. Braking ellipses aggravate the guidance problem and lift inside the atmosphere aggravates the total heat problem though it would not increase the peak heating rate. Neither of these problems have yet been solved, so it may be idle to speculate on which is the more impossible. High temperature sublimation and ablation materials have appeared on the horizon, whereas the same cannot be said of lunar guidance equipment.

Of course it will be necessary to supply guidance to reach the correct re-entry point in either case. For instance, the listed tolerance of 0.1° in the re-entry angle corresponds to a difference of only 6,800 feet in the perigee which the orbit would have in the absence of any atmosphere. In other words, the guidance system would be required to control the hypothetical perigee or distance of closest approach to this ac curacy. The perigee would occur, incidentally belo 200,000 feet, depending on the re-entry angle use For braking ellipses, it would appear that this accura would have to be supplied, not once, but several time and uncertainties in atmospheric density would b quite serious.

Nomenclature

D	Drag
K	Constant, Equation (2)
$\bar{K}$	Reciprocal of Body Nose Radius
L	Lift
L_E	Lewis Number
Q_a	Aerodynamic Heat Input
$\dot{Q}_a$	Aerodynamic Heating Rate
R	Body Nose Radius
R_E	Mean Earth Radius
g	Gravitational Acceleration at Earth's Surfac
h	Altitude above the Earth
$\bar{h}$	Gas Enthalpy
$\bar{h}_D$	Average Dissociation Energy per Unit of Mas
j	Joule's Constant
k	Density Ratio Across the Shock
q	Dynamic Pressure
$\frac{SC_D}{m}$	Drag Parameter
$\frac{SC_L}{m}$	Lift Parameter
U	Velocity
$\frac{2R}{U_\infty}\left(\frac{du}{dx}\right)_s = F(k)$	Non-dimensional Stagnation Poi Gradient
γ	Flight Path Angle
θ	Negative Flight Path Angle
ϕ	Range from Re-entry
ρ	Air Density
μ	Viscosity Coefficient
δ	Shock Layer Thickness

Subscripts

s	Stagnation Point
w	Body Wall
∞	Free-Stream

References

[1] Allen, H. and A. J. Eggers, Jr. *A Study of the Moti and Aerodynamic Heating of Missiles Entering t Atmosphere at High Supersonic Speeds* NACA T 4047, 1957 (Supersedes NACA RM A53D28).

[2] *NACA Conference on High-Speed Aerodynamics*, Am Aeronautical Laboratory, Moffett Field, Calif. 18– March 1958. There are many papers here on aspec of the satellite re-entry problem, principally those Chapman; Faget, Garland and Buglia; Wong, He mach, Reller and Tinling; Becker.

[3] Gazley, Carl, Jr. *The Penetration of Planetary A mospheres* Rand Report P-1322, 24 February 1958.

4] A. C. Robinson and Frank Niuman.—*On the Representation of Dynamic Pressure in Analog Simulations Involving Large Changes in Atmospheric Density*—WADC TN 58-209, August 1958.

5] Rose, P. H. and Stark, W. I. *Stagnation Point Heat Transfer Measurements in Dissociated Air*, J. AERONAUTICAL SCIENCES, February 1958.

6] Fay, J. A. and Riddell, J. R. *Theory of Stagnation Point Heat Transfer in Dissociated Air*, J. AERONAUTICAL SCIENCES, February 1958.

7] Ting Yi Li. *Inviscid Flow Field Around a Blunt Body at Hypersonic Speeds, Part I, The Stagnation Point Region*—TR AF-5706, Renselear Polytechnic Institute, September 1957.

[8] Feldman, Saul. *Hypersonic GHS Dynamic Charts for Equilibrium Air*, AVCO Res. Lab. January 1957.

[9] Gilmore, F. R. *Equilibrium Composition of Thermodynamic Properties of Air to 24,000° K* RM-1543, Project Rand, August 1955.

[10] Hansen, C. Fredrick. *Approximations for the Thermodynamic and Transport Properties of High Temperature Air*, NACA TN 4150, 1958.

[11] Blanch, Gertrude, et al. *Tables of Sine, Cosine, and Exponential Integrals*, Volume I, National Bureau of Standards.

[12] Comrie, L. J., *Chambers' Shorter Six-Figure Mathematical Tables*, W. R. Chambers, Ltd., London, 1955.

[13] Peirce, B. O. *A Short Table of Integrals*, Ginn and Company, New York, 1929.

Technical Notes

Dual Burning Propulsion Systems for Satellite Stages

B. P. Martin*

bstract

A satellite vehicle system whose last stage can be shut down and restarted is shown by basic energy relationships to have a decided performance advantage over a vehicle system which is identical except for having only the conventional one-shot capability. For an assumed final stage weight and boost ascent, curves of payload vs. orbit altitude are derived and compared for the two final stage thrust systems.

ntroduction

Except for effects of gravity and drag, a given impulse irected along the velocity vector of a mass will result in the ame velocity change of the mass for all values of original elocity of the mass. But since kinetic energy varies as the quare of the velocity magnitude, the energy change for a ven impulse increases with increasing values of original elocity. There is, therefore, an advantage, from the standpoint of minimizing rocket propellant required, in supplying much of the total impulse as possible when the velocity the rocket is high; i.e., when the energy of the rocket is rgely in kinetic form. Ideally then, all of the energy reuired for a particular satellite orbit should be supplied just bove the atmospheric drag regions, whereupon the vehicle oves on a frictionless track into a horizontal trajectory at e proper altitude. Since these frictionless tracks are not nder development, the next best technique must be emoyed. In this technique, as little impulse as possible is left be supplied under conditions of reduced velocity and high titude and is accomplished by having the begin-coast titude as low as practical and the begin-coast velocity as gh as possible consistent with the final altitude desired. he limiting value for this velocity is that for perigee of an cent ellipse whose apogee altitude is essentially that of the sired final orbit.

ual Burning Concept

For good staging ratios, however, a stage break probably ll not be indicated at perigee, in which case only the apogee locity increment would be supplied by the final stage.

* Staff Scientist, Spacecraft Dept., Lockheed Missiles & ace Division.

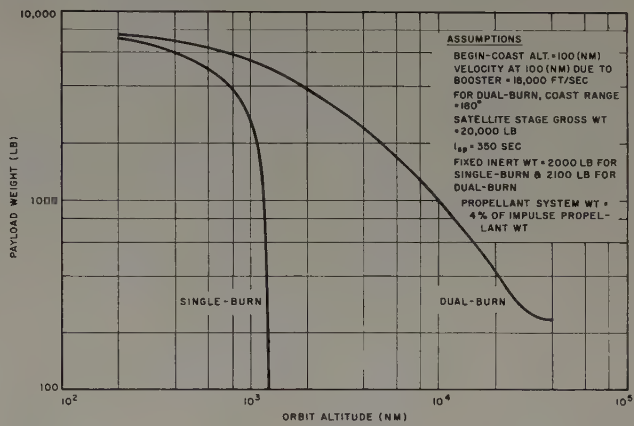

Fig. 1. Payload vs. Orbit Altitude

For most Earth satellite orbit altitudes and vehicle configurations, high staging efficiency will call for the final stage to assume a greater part of the overall velocity requirement (frequently referred to as characteristic velocity) than the velocity increment required at apogee. These ascent and performance criteria led to consideration of two periods of thrust for the final orbiting stage; i.e., "dual burning", in order to arrive on the coasting ellipse near perigee while an efficient stage distribution of the total velocity requirement is maintained.

The more conventional single-burn trajectories and dual-burn trajectories may be summarized for comparison as follows:

(1) *Single-Burn Ascent Trajectory*—At burnout of the boost stage, or stages, the flight path angle is such that for the speed and altitude attained, the coast phase which follows will carry the vehicle to apogee which is essentially equal to the final orbit altitude. Just prior to apogee the final stage propulsion system is operated to provide orbit injection.

(2) *Dual-Burn Ascent Trajectory*—At burnout of the boost stage, or stages, the flight path angle and altitude are, in general, lower than for the single-burn case. Immediately after booster separation, the final stage propulsion system is operated long enough to increase the speed essentially to perigee speed for an ascent ellipse whose apogee is at the altitude of the desired orbit. After a long coast (through a range angle of up to 180 degrees) the propulsion system is

restarted and operated long enough to bring the speed up to orbital speed.

As mentioned earlier, total velocity requirements are lowest for a coast range of 180 degrees (coast begins at perigee) because this permits the highest begin-coast speed. However, the effect on the total velocity requirement of reducing coast range from this value is rather slight until coast range is substantially reduced. Therefore, the exact coast range for a particular mission should be selected after including other considerations such as guidance component errors for various coast times, sensitivity ranges of radiation sensors if used in the ascent guidance system, and propellant boil-off during coast. For the performance comparison of single-burning and dual-burning which is presented herein, a coast range of 180 degrees was assumed for the dual-burning case.

For both cases energy is conserved during the coasting ellipse, so that the vehicle velocity at the end of the coast period may be found from the kinetic and potential relationship as follows:

$$\frac{V_1^2}{2} - \frac{GM}{r_1} = \frac{V_2^2}{2} - \frac{GM}{r_2} \tag{1}$$

where: V_1 = velocity at beginning of coast
r_1 = length of radius vector at beginning of coast
GM = the product of the universal gravitational constant into Earth's mass, taken as 1.4077 $\times 10^{16}$ ft^3 sec^{-2}
V_2 = velocity at end of coast
r_2 = length of radius vector at end of coast

or

$$V_2 = \sqrt{V_1^2 - 2GM\frac{r_2 - r_1}{r_2 r_1}} \tag{2}$$

It was assumed for the example that the satellite stage gross weight and the booster vehicles are identical for both types of trajectories, and that the mission calls for a circular orbit at 1000 nautical miles altitude.

Booster burnout for the single-burn vehicle was assumed to occur at 100 nautical miles altitude at a velocity of 18,000 ft/sec and for the dual-burn vehicle, at a somewhat lower altitude (due to the flatter trajectory) but with the same total energy.

Single-Burn Performance

After booster burnout, the single-burn vehicle coasts on a constant energy ellipse to apogee at 1000 nautical miles. The begin-coast conditions coincide with the booster burnout conditions. The velocity at the end of the coast period is found from Eq. 2 as:

$$V_2 = 7650 \text{ ft/sec.}$$

The required orbital velocity at 1000 nautical miles is 22,850 ft/sec. The velocity differential, or Δv, that must be supplied by the vehicle then is 22,850 − 7650 = 15,200 ft/sec.

Dual-Burn Performance

In the case of dual burning, the boost phase is immediately followed by the first of two separate thrust phases. The desired velocity (perigee velocity) at the end of this first burning phase for a coast range of 180 degrees may be found from:

$$V_P = \sqrt{2GM\left[\frac{r_A}{r_P(r_P + r_A)}\right]} \tag{3}$$

where: V_P = velocity at perigee
r_A = apogee radius = Earth's radius + 1000 n.m.
r_P = perigee radius

The value of r_P depends upon the individual vehicle and trajectory characteristics. For this example assume that the altitude at the end of the first burning phase, and the beginning of the coast phase (perigee), is again 100 nautical miles. Since the total energy at booster burnout was assumed to be equivalent to that for single burning, the velocity increment for the first burning phase can be taken as the difference between the perigee velocity and 18,000 ft/sec.

This is a rather conservative approach for two reasons, viz.: (1) Since the boost trajectory will be somewhat flatter for dual burning, gravity losses will be lower and burnout energy will be higher in spite of slightly increased drag losses; (2) the first burning velocity increment is actually accumulated over the altitude change from booster burnout to begin coast which (because the impulse is furnished at a more favorable kinetic-potential energy distribution) is more efficient than the assumed instantaneous burning at begin coast altitude.

For the assumed 100 n.m. perigee, perigee velocity, from Eq. 3 is:

$$V_P = 26{,}990 \text{ ft/sec.}$$

The velocity increment to be supplied during first burn is then:

$$\Delta V_1 = V_P - 18{,}000 = 8990 \text{ ft/sec.}$$

The velocity after coasting to 1000 n.m. may be found (by conservation of energy) from Eq. 2, or, by conservation of angular momentum:

$$V_A = V_P[r_P/r_A] \tag{4}$$

$$V_A = 21{,}520 \text{ ft/sec.}$$

The velocity increment required at apogee during the second burning period is then:

$$\Delta V_2 = 22{,}850 - V_A = 1330 \text{ ft/sec.}$$

The total satellite stage velocity increment required for dual burning is:

$$\Delta V_1 + \Delta V_2 = 10{,}320 \text{ ft/sec.}$$

Payload Comparison for Single-burning and Dual-burning Stages

The above velocity requirement of 10,320 ft/sec. is compared with 15,200 ft/sec. required for single burning. The difference in final stage velocity requirements can be converted into payload differential for a given final stage gross weight and known characteristics of the propulsion system and other subsystems. This velocity-to-payload conversion was computed for the boost ascent assumed herein for several orbit altitudes based upon a satellite stage gross weight of 20,000 lb. and specific impulse of 350 seconds. Payload weight was assumed to be related to burnout weight by the following expression:

$$W_{PL} = W_{BO} - 2000 - 0.04W_P - X \tag{5}$$

where: W_{PL} = weight of payload
W_{BO} = weight at burnout = $20{,}000e^{-(\Delta V/350g)}$
W_P = weight of impulse propellant required
X = zero for single-burning and 100 lb. for dual burning to cover second start requirement

The results are compared in Fig. 1. The boost trajectory d payload expression, although greatly simplified, serve show that substantial payload increases are available. ie abrupt decrease in payload for the single-burn curve is e to the rapid increase (to vertical) for the begin-coast ght path angle to achieve the indicated altitude at apogee.

The maximum altitude obtained for the above assumptions with single burning was found to be 1265 n.m. For this altitude, since the ascent must be vertical, apogee velocity is zero and the velocity increment required is the entire orbit velocity.

Anisotropy of Escape Velocity from the Moon, the Lunar Atmosphere and the Origin of Craters

Louis Gold*

ostract

A simple estimate for the degree of anisotropy to be expected in the lunar escape velocity owing to the earth's gravitational field provides a basis for assessing the role of directed streaming of the moon's atmosphere—the lunar wind—as it might have contributed to the genesis of craters. The constant aspect of the moon (relative to the earth) might have provided the essential orienting effect in the formation of the ordered appearance of the lunar craters during its primordial evolution. The possible connection of the streaming ionized residual atmosphere of the moon with a predicted weak but decidedly anisotropic lunar magnetic field is pointed out. Thus the ideal launching positions for return flights to earth may have to allow for dangerous radiation belts encircling the moon as well as minimal propulsion requirements.

scussion

It was pointed out some time ago [1] that the strong anitropy of the escape velocity from the surface of the moon ght have a bearing on the formation and general aparance of the lunar craters. This brief note is intended to borate somewhat on such an hypothesis and its conquences. The imminence of lunar landings and exploration ikes it of practical import to report on the following theoical considerations. Recent accounts of volcanic activity the moon have also stimulated current interest in the ystery of the lunar craters [2].

While the restricted three body problem as solved in the m of the Jacobi integral does imply an anisotropy of the ape velocity from the moon, this has not been generally preciated. Moreover, no actual calculation of this effect has parently been made. Since the Jacobi solution fails to orporate many other possible contributions to the lunar ape such as the asphericity of the earth and moon, solar rturbation, etc., the approximation derived earlier [3]

$$\frac{1}{2}(v^2 - v_0^2) = G\left(\frac{M_1}{r} \pm \frac{M_2}{d \pm r}\right) + G\left(\frac{M_2}{d \pm r_0} \pm \frac{M_1}{r_0}\right) \quad (1)$$

y be employed for this purpose. Here at time $t = 0$ the tial velocity $v = v_0$ and M_1, M_2 denote the respective isses of the moon and earth; d is the distance between the nters of M_1 and M_2 with r_0 the lunar radius, etc. The sign propriately must be chosen according to whether flights ginate on the near or far side.

Escape for the latter case corresponds to $v = 0$ as $r \to \infty$, ereby

$$(V_E^2)_{F.S.} = 2G\left(\frac{M_1}{r_0} + \frac{M_2}{d + r_0}\right) = 2g_0 r_0\left(1 + \frac{M_2}{M_1}\cdot\frac{r_0}{d + r_0}\right) \quad (2a)$$

in which g_0 represents the conventional gravitational constant referred to the moon's surface. On the other hand, for the near side, the escape velocity V_E associates with $r = r_E = d(1 + M_2/M_1)^{-1}$, whence

$$(V_E^2)_{N.S.} = 2G\left(\frac{M_1}{r_0} - \frac{M_2}{d - r_0}\right) = 2g_0 r_0\left(1 - \frac{M_2}{M_1}\cdot\frac{r_0}{d + r_0}\right) \quad (2b)$$

If the true neutral point is introduced

$$d_n = d\left(1 + \sqrt{\frac{M_2}{M_1}}\right)^{\frac{1}{2}} \quad (3a)$$

a somewhat altered expression for (2b) arises

$$(V_E^2)_{N.S.} = 2G\left\{M_1\left(\frac{1}{r_0} - \frac{1}{d - d_n}\right) + M_2\left(\frac{1}{d - r_0} - \frac{1}{d_n}\right)\right\} \quad (3b)$$

As only an approximate estimate is involved here anyway, the similarity of form in (2a) and (2b) permits easy insight as to how the ratio $(V_E)_{N.S.}/(V_E)_{F.S.}$ depends upon the masses and distances in the domain of interest.

Numerically then the simple calculation

$$\frac{M_2}{M_1}\cdot\frac{r_0}{d + r_0} \cong 0.34$$

leads to the ratio

$$\frac{(V_E)_{N.S.}}{(V_E)_{F.S.}} = \left(\frac{1 - 0.34}{1 + 0.34}\right)^{\frac{1}{2}} = 0.70$$

which demonstrates the significant role played by the earth in influencing flights leaving from the moon. But another factor which has to do with ideal launch from our satellite concerns the possibility of lunar radiation belts, an aspect to be entered into later.

The severe anisotropy of the escape velocity which has now been characterized may have exerted an important influence on the origin of the lunar crater pattern. It may be conjectured that while the moon's surface was in a semi-plastic state during its evolutionary phase with hot gas issuing from its interior, the severe streaming of the atmosphere produced huge whirls which were eventually frozen in upon final solidification. The oriented streaming, maintained by the constant aspect of the moon presented to the earth, would tend to induce some sort of ordered appearance of the resultant craters: the meteor impact hypothesis hardly accounts for the general appearance. The craters of Tycho and Copernicus

* Radiation, Inc., Research Division, Orlando, Florida. Present address: Project Matterhorn, Princeton Univery, Princeton, New Jersey.

are excluded from this picture as they may have been formed by meteor bombardment as suggested by the star-like rays surrounding them which have been ascribed to the settlement of meteoric dust in the moon's gravitational field [4].

The primordial streaming must likely have been typical of mach flow in the hypersonic regime. While the present receding position of the moon may considerably moderate the streaming action, it is possible that the greatly reduced density of the lunar atmosphere may yet be conducive for a high degree of ionization. Thus, apart from the question of concentrating the craters at the periphery of the lunar disc which corresponds to the observed situation, there is then the implication of a highly ionized residual lunar atmosphere. Failure to detect the moon's atmosphere by close passage of radiation from a star may in some way be due to the peculiarities of such a streaming, ionized sheath.

At this juncture, there arises the suggestion of highly anisotropic magnetic fields surrounding the moon; a lunar wind of the character described above has its evident counterpart of solar winds [5]. The prediction is made that the moon will be found to possess a weak but strongly oriented magnetic fiel The question of charge particle trapping naturally follow and so the possibility of lunar radiation belts may need to b appraised, particularly with regard to the contemplate manned landings. More detailed theoretical development along these lines are in progress.

References

[1] Gold, L. *Earth-Moon Rocket Trajectories*; paper presente at the American Rocket Society meetings, June, 195 Los Angeles.

[2] Kopal, Z. *Origin of the Lunar Craters and Maria*; Natur 183, 169 (1959). See also W. G. Van Dorn and Z. Kopa Nature 183, 737–738 (1959), on same subject.

[3] Gold, L. *Earth-Moon Rocket Trajectories*; J. Frankli Inst. 266, 1 (1958).

[4] Urey, H. C. *The Planets*; New Haven, Yale Press, 195

[5] Gold, L. *Gravitational-Magnetic Origin of Sunspots an Related Phenomena*; paper presented at the I. A. F. Co gress, September, 1959, London.

Format of Technical Papers for AAS Journal

The editors will appreciate the cooperation of authors in using the following directions for the preparation of manuscripts. These directions have been compiled with a view toward eliminating unnecessary correspondence, avoiding the return of papers for changes, and reducing the charges made for "author's corrections."

Manuscripts

Papers should be submitted in original typewriting (if possible) on one side only of white paper sheets, and should be double or triple spaced with wide margins. However, good quality reproduced copies (e.g. multilith) are acceptable. An additional copy of the paper will facilitate review.

Company Reports

The paper should not be merely a company report. If such a report is to be used as the basis for the paper, appropriate changes should be made in the title page. Lists of figures, tables of contents, and distribution lists should all be deleted.

Titles

The title should be brief, but express adequately the subject of the paper. A footnote reference to the title should indicate any meeting at which the paper has been presented. The name and initials of the author should be written as he prefers; all titles and degrees or honors will be omitted. The name of the organization with which the author is associated should be given in a separate line to follow his name.

Abstracts

An abstract should be provided, preceding the introduction, covering contents of the paper. It should not exceed 200 words.

Headings

The paper can be divided into principal sections as appropriate. Headings or paragraphs are not numbered.

Mathematical Work

As far as possible, formulas should be typewritten. Greek letters and other symbols not available on the typewriter should be carefully inserted in ink. Each such symbol should be identified unambiguously the first time it appears. The distinction between capital and lower-case letters should be clearly shown. Avoid confusion between zero (0) and the letter O; between the numeral (1), the letter l, and the prime ($'$); between alpha and a, kappa and k, mu and u, nu and v, eta and n.

The level of subscripts, exponents, subscripts to subscripts, and exponents in exponents should be clearly indicated.

Complicated exponents and subscripts should be avoided when possible to represent by a special symbol.

Fractions in the body of the text and fractions occurring in the numerators or denominators of fractions should be written with the solidus. Thus

$$\frac{\cos(\pi x/2b)}{\cos(\pi\alpha/2b)}$$

is the preferred usage.

The intended grouping of handwritten formulas can be made clear by slight variations in spacing, but this procedure is not acceptable in printed formulas. To avoid misunderstanding, the order of symbols should therefore be carefully considered. Thus

$(a + bx) \cos t$ is preferable to $\cos t\,(a + bx)$

In handwritten formulas the size of parentheses, brackets and braces can vary more widely than in print. Particular attention should therefore be paid to the proper use of parentheses, brackets, and braces (which should be used in this order). Thus

$$\{[a + (b + cx)^n] \cos ky\}^2$$

is required rather than $((a + (b + cx)^n) \cos ky)^2$.

Equations are numbered and referred to in text as (15).

Illustrations

Drawings should be made with black India ink on white paper or tracing cloth, and should be at least double the desired size of the cut. Each figure number should be marked with soft pencil in the margin or on the back of the drawing. The width of the lines of such drawings and the size of the lettering must allow for the necessary reduction. Reproducible glossy photographs are acceptable. However, drawings which are unsuitable for reproduction will be returned to the author for redrawing. Legends accompanying the drawings should be typewritten on a separate sheet, properly identified.

Bibliography

References should be grouped together in a bibliography at the end of the manuscript. References to the bibliography should be made by numerals between square brackets [4].

The following examples show the approved arrangements:

for books—[1] HUNSAKER, J. C. and RIGHTMIRE, B. S., *Engineering Applications of Fluid Mechanics*, McGraw-Hill Book Co., New York, 1st ed., 1947, p. 397.

for periodicals—[2] Singer, S. F., "Artificial Modification of the Earth's Radiation Belt," *J. Astronaut. Sci.*, *6* (1959), 1–10.